Remote Sensing of Environment 240 (2020) 111676

Contents lists available at ScienceDirect

Remote Sensing of Environment

journal homepage: www.elsevier.com/locate/rse

Fluorescence Correction Vegetation Index (FCVI): A physically based reflectance index to separate physiological and non-physiological information in far-red sun-induced chlorophyll fluorescence

Peiqi Yang[a,*], Christiaan van der Tol[a], Petya K.E. Campbell[b,c], Elizabeth M. Middleton[c]

[a] Faculty of Geo-Information Science and Earth Observation (ITC), University of Twente, Enschede 7500 AE, the Netherlands
[b] Joint Center for Earth Systems Technology (JCET), University of Maryland, Baltimore County, Baltimore, MD 21228, USA
[c] Biospheric Sciences Laboratory, NASA Goddard Space and Flight Center, Greenbelt, MD 20771, USA

ARTICLE INFO

Keywords:
Chlorophyll fluorescence
Vegetation reflectance index
Canopy structure
Sun-observer geometry
Photosynthesis
Spectral invariants

ABSTRACT

Sun-induced chlorophyll fluorescence (SIF) has been used to track vegetation photosynthetic activity for improving estimation of gross primary productivity (GPP) and detecting plant stress. There are both physical and physiological controls of SIF measured at the surface and retrieved from remote sensing including satellite observations. In order to accurately use SIF for monitoring of plant physiology, the effects of physically-based radiation processes related to leaf and canopy structure, notably photosynthetically active radiation (PAR) absorption and SIF scattering and re-absorption, must be characterized. In this study, we investigate both PAR absorption and SIF scattering processes and find that although it is difficult to quantify their effects individually by using just reflectance, the combined effects of the two processes can be well approximated by a reflectance index. This index, referred to as FCVI (Fluorescence Correction Vegetation Index), is defined as the difference between near-infrared (NIR) and broad-band visible (VIS, 400–700 nm) reflectance acquired under identical sun-canopy-observer geometry of the SIF measurements. The development of the index was based on the physical connection between reflectance and far-red SIF, which was revealed by using the spectral invariant theory. The utility of FCVI to correct far-red SIF for PAR absorption and scattering effects, thus improving the link to photosynthesis, was tested with data from: (i) a field experiment for a growing season; and (ii) a numerical experiment which included a number of scenarios generated by a radiative transfer model. For both the observations and simulations, the FCVI provided a promising estimate of the impact of the physically-based radiation processes on far-red SIF of moderately dense canopies (i.e., FCVI $\geq$ 0.18). Normalizing the TOC far-red SIF by both the incident PAR (iPAR) and the FCVI provided a good estimate of the far-red fluorescence emission efficiency of the canopies examined. This approach enhances our ability to generalize retrievals for vegetation processes as they change through natural growth phases and seasons. Taken together, far-red SIF and FCVI may enable the assessment of the light partitioning of vegetation canopies, an essential step to facilitate the use of far-red SIF for tracking physiological processes.

1. Introduction

Remote sensing of sun-induced chlorophyll fluorescence (SIF) is becoming a frequently used technique in plant physiology monitoring as a non-invasive measurement of canopy photosynthetic activities. Top-of-canopy (TOC) SIF is the final outcome of three sequential processes: absorption of sunlight by chlorophyll followed by fluorescence emission by photosystems, and both re-absorption and scattering after this emission. Among these processes, the emission of leaf-level fluorescence is regulated by a number of physiological mechanisms and describes the partitioning of photosynthetically active radiation (PAR) into photosynthesis, heat dissipation and fluorescence and by using pulse-amplitude-modulation (PAM) techniques one can derive the partitioning (Baker, 2008; Maxwell and Johnson, 2000; Middleton et al., 2018). Because of the sensitivity of TOC SIF to physiological processes, SIF observed with remote sensing tools has been used to infer photosynthetic capacity (Zhang et al., 2014), improve gross primary production (GPP) estimation (Campbell et al., 2019; Guanter et al., 2014; Migliavacca et al., 2017), reveal vegetation stress (Ač et al., 2015; Rossini et al., 2015), and estimate transpiration (Lu et al., 2018; Shan

* Corresponding author.
E-mail address: p.yang@utwente.nl (P. Yang).

https://doi.org/10.1016/j.rse.2020.111676
Received 23 May 2019; Received in revised form 17 December 2019; Accepted 21 January 2020
Available online 31 January 2020

et al., 2019).

The potential of SIF for plant physiology monitoring has not been fully explored. A substantial portion of the SIF variations observed at different spatial and temporal scales are due to variations in vegetation biochemical constituents as well as leaf and canopy structure, rather than changes in plant physiology (Migliavacca et al., 2017; Van der Tol et al., 2016). Consequently, extracting physiological information from SIF presents a challenge because the SIF signal suffers from the interferences caused by PAR absorption and SIF scattering into the viewing direction, which are controlled by physical factors, such as soil background, leaf biochemical constituents, canopy structure and sun-observer geometry. Prior investigations have shown that both TOC SIF and GPP are largely explained by vegetation structure (Badgley et al., 2017, 2018) and the positive correlation between SIF and GPP can be dominated by light absorption process rather than the functional link at photosynthetic level (Miao et al., 2018; Yang et al., 2018).

One way to examine the effects of PAR absorption and SIF scattering on TOC SIF is to employ radiative transfer models (RTMs), which explicitly simulate light interactions with canopies based on physical laws, and link soil and vegetation properties with TOC SIF. RTMs have provided valuable tools for understanding of the sensitivity of SIF to its controls. For example, Verrelst et al. (2015) carried out a sensitivity analysis with the 1-D RTM SCOPE (Soil Canopy Observation, Photochemistry and Energy fluxes, Van der Tol et al., 2009) and ranked the effects of canopy structure, leaf pigment content and photosynthetic capacity on TOC SIF at different wavelengths. Similarly, Hernández-Clemente et al. (2017) used a 3-D RTM to successfully estimate the structural effects of forest canopy on TOC SIF measurements and demonstrated the significance of these effects. Furthermore, Celesti et al. (2018) used SCOPE to explore physiological information related to SIF and found that fluorescence emission efficiency increased when photosynthesis was inhibited. Despite the powerful capabilities of RTMs, their usage in quantifying the impact of physiological and physical processes may not be practical in many cases, since RTMs require prior information about canopy structure and leaf properties which are often unknown (Porcar Castell et al., 2014).

Reflectance provides valuable information for interpreting SIF measurements. In two earlier studies, we used reflectance to estimate leaf and canopy properties by model inversion (Van der Tol et al., 2016; Yang et al., 2019). After these properties were estimated, their effects on TOC SIF were evaluated through characterizing the light absorption and SIF scattering processes, predicted with RTMs. However, the estimation of vegetation canopy parameters by model inversion requires multi-spectral or preferably hyperspectral reflectance rather than reflectance at two or three bands (e.g., reflectance indices) (Verrelst et al., 2019). Both the model inversion and simulation of SIF radiative transfer are computationally expensive and have limits in large-scale applications. Apart from these limitations, the model inversion is typically ill-posed and there are uncertainties in the estimated vegetation properties, which may be propagated to the estimated effects of the light absorption and SIF scattering processes (Yang et al., 2019).

In contrast to the explicit RTMs, a simple light use efficiency (LUE) model has been formulated to incorporate the effects of the three processes acting on TOC SIF. The formulation takes the form of the LUE concept in GPP estimation (Monteith, 1972), which defines the intensity and spectral properties of a TOC SIF signal observed by a remote sensor as:

$$F_{toc} = \mathrm{iPAR} \times \mathrm{fAPAR}_{chl} \times \epsilon_F \times \sigma_F \quad (1)$$

where iPAR denotes the available incident PAR for a canopy, fAPAR_{chl} is the fraction of absorbed PAR (APAR) by chlorophyll, which is often approximated by fAPAR (i.e., the fraction of PAR absorbed by the entire canopy not just chlorophyll). ϵ_F is canopy SIF emission efficiency and σ_F is the scattering of SIF in the viewing direction, also known as fluorescence escape probability p_{esc} or escape fraction f_{esc} (Guanter et al., 2014) (i.e., $\sigma_F = f_{esc} = p_{esc}$ and $0 \le \sigma_F \le 1$ due to re-absorption). In this expression, the impacts of PAR absorption, SIF emission and SIF scattering are quantified by fAPAR_{chl} (or fAPAR), ϵ_F and σ_F, respectively.

Based on Eq. (1), a number of practical approaches to correct for the impact of the physical processes on SIF have been explored. Normalizing TOC far-red SIF by canopy APAR (i.e., the product of fAPAR and iPAR) has been commonly used to account for the variation in the light availability and absorption process to allow the exploration of the link between the SIF/APAR ratio and photosynthesis, an approach that has met with varying success. For example, at a local scale, Yang et al. (2015) measured APAR of a temperate deciduous forest by using a set of quantum sensors and found that the far-red SIF/APAR ratio was positively correlated with photosynthetic LUE, while Miao et al. (2018) found that this ratio was negatively correlated with photosynthetic LUE of a soybean field. Wieneke et al. (2018) reported that more than 50% of the observed diurnal and seasonal variation of photosynthetic LUE can be explained by this ratio, but they also found an even stronger relationship between the far-red SIF/APAR ratio and a structural vegetation index. Yoshida et al. (2015) computed APAR from MODIS fAPAR products and found GOME-2 SIF products normalized by APAR clearly declined over the region impacted by the 2010 Russian heat wave, while Wohlfahrt et al. (2018) showed that SIF had limited potential for quantitatively monitoring photosynthesis during heat waves in the absence of large changes in APAR (i.e., variations due to the efficiency ϵ_F). The inconsistent findings between the far-red SIF/APAR ratio and photosynthetic LUE are at least partly caused by the fact that normalizing SIF measurements for APAR results in a signal that is still contaminated by canopy structural effects due to the variations in SIF scattering. Without considering the scattering process, the ‘ pure’ physiological information (i.e., ϵ_F) cannot be completely separated from the structural and illumination effects. Our goal and challenge are to isolate the physiological parameter ϵ_F from fAPAR and σ_F (Eq. (1)) to obtain reliable physiological status information of vegetation.

Attempts to correct SIF for the effects of scattering (σ_F) to achieve a better physiological indicator have been made in recent years. He et al. (2017) performed angular normalization of TOC SIF and partially corrected the variation of σ_F caused by different viewing angles. They found that such normalization provided a better proxy of GPP as compared to the use of SIF uncorrected for angular scattering. Recently, we linked σ_F of far-red SIF with TOC near-infrared (NIR) reflectance by comparing the radiative transfer of incident radiation and emitted SIF (Yang and Van der Tol, 2018). We found that for dense vegetation canopies, σ_F was proportional to NIR reflectance and to the reciprocal of canopy interceptance (i_0) (i.e., $\sigma_F = R_{nir}/i_0$), which is the portion of the incident photons that interact with the canopy (see Smolander and Stenberg, 2005, and Section 2.1) . Liu et al. (2018) utilized this link and estimated σ_F from TOC reflectance by using a machine learning approach. By normalizing the TOC SIF by this estimated value for σ_F, they obtained an estimate for canopy total emitted far-red SIF. Although there is a strong connection between TOC reflectance and far-red SIF, the estimation of σ_F from reflectance only is still to be resolved because the estimation requires canopy interceptance knowledge apart from TOC reflectance (Yang and Van der Tol, 2018).

Zeng et al. (2019) extended the relationship between σ_F and NIR reflectance to sparse vegetation canopies and proposed to use the NDVI (normalized difference vegetation index, Rouse et al., 1973) to approximate the contribution of ‘ pure’ vegetation signals. They derived σ_F as the ratio of the product of NIR reflectance and NDVI to i_0 (i.e., $\sigma_F = R_{nir} \times \mathrm{NDVI}/i_0$). Furthermore, Zeng et al. (2019) proposed to use fAPAR to approximate i_0 for practical usage and obtained $\sigma_F = R_{nir} \times \mathrm{NDVI}/\mathrm{fAPAR}$. Using this expression of scattering of far-red SIF, we can estimate the product of fAPAR and σ_F as $R_{nir} \times \mathrm{NDVI}$ straightforwardly. A limitation of this approach is that a number of steps in the derivation for σ_F are not fully consistent with radiative transfer theory, and therefore are not universally valid. For example, 1) the use of NDVI as a measure for ‘ pure’ vegetation signals could be debated as NDVI is still dependent on the soil spectrum to some degree, 2) fluorescence

excited by scattered radiation is not considered, and 3) using fAPAR for the spectral invariant i_0 relies on the assumption that both soil and leaves are perfectly absorbant (i.e., leaf albedo and soil reflectance are both zero). Furthermore, the accurate estimation of fAPAR is difficult and thus additional errors may be introduced in the estimation of σ_F when implementing that approach in practice.

Direct fAPAR or APAR measurements are not commonly available, especially for global applications. Most remote sensing fAPAR products are derived from the canopy reflectance signal, but the use of canopy reflected signals to estimate canopy absorbed signals (i.e., fAPAR or APAR) is an ill-posed problem as the relationship between fAPAR and reflectance is regulated by canopy transmittance and soil absorptance. For example, the use of reflectance indices (e.g., EVI and NDVI) to estimate fAPAR (preferably $fAPAR_{chl}$) is possible (Viña and Gitelson, 2005), even globally (Huete et al., 2002; Myneni et al., 2002), but the empirical coefficients for the reflectance index approach are limited to specific cases (e.g., a regional area and/or at a specific period).

In this study, we evaluate the possibility to link fAPAR to TOC reflectance analytically, since far-red σ_F has already been related to TOC NIR reflectance in our previous study (Yang and Van der Tol, 2018). We demonstrate that although it is difficult to estimate fAPAR and far-red σ_F individually by using just TOC reflectance, their product can be well approximated by a reflectance index. The new reflectance index (i.e., Fluorescence Correction Vegetation Index, FCVI) is given as the difference of NIR and broadband visible (VIS) reflectance acquired under identical sun-canopy-observer geometry of the SIF measurements. In what follows, we develop the theoretical basis for FCVI, which is based mainly on the spectral invariant radiative transfer theory (Huang et al., 2007; Knyazikhin et al., 2011; Lewis and Disney, 2007; Stenberg et al., 2016). Further, we evaluate the utilities of the FCVI by using field measurements of a corn canopy and simulations from the RTM SCOPE. Our objective is to improve estimation performance for the physiological information captured with far-red SIF, by reducing the influence of physical processes that contaminate the observed SIF signal.

2. Theoretical basis

In this section, we present: 1) an overview of the spectral invariant theory and its usage in parametrizing canopy scattering (s), absorption (a) and TOC reflectance (R); 2) the application of this theory to estimate far-red σ_F and review the connection between far-red σ_F and TOC NIR reflectance; 3) an expression for fAPAR as a function of TOC reflectance using the implicit connection between canopy absorption and TOC reflectance; and 4) the derivation of the product of fAPAR and far-red σ_F, which represents the combined effects of PAR absorption and SIF scattering. We define this product as the ‘ radiative transfer factor’ (Γ_{rt} = fAPAR × σ_F) since it represents the combined effects of two radiative transfer processes on TOC SIF.

The proposed far-red fluorescence correction vegetation index (FCVI) to serve as a surrogate for the radiative transfer factor (Γ_{rt}) is defined as:

$$\mathrm{FCVI} = R_{nir} - R_{\overline{vis}} \tag{2}$$

where R_{nir} is directional reflectance at the NIR plateau stretching approximately from 750 nm to 900 nm, close to the spectral band of interest for far-red SIF (e.g., SIF at 760 nm). $R_{\overline{vis}}$ is the broadband visible (VIS) directional reflectance over the 400–700 nm range of PAR. It is important to note that an identical sun-canopy-observer geometry between TOC far-red SIF and reflectance acquisition is a mandatory condition for applying the FCVI approach to estimate Γ_{rt}. Otherwise, the connections between NIR reflectance and far-red SIF scattering, and between reflectance and PAR absorption described below are not valid.

2.1. Overview of the spectral invariant theory

The spectral invariant approach allows for a very accurate parametrization of the canopy scattering s, absorption a, TOC directional reflectance R by using the wavelength dependent leaf albedo ω (i.e., the sum of leaf reflectance and transmittance), and three spectrally invariant and structurally varying parameters: canopy interceptance i_0, recollision probability p and directional escape probability $\rho(\Omega)$, where Ω indicates the viewing direction.

The theory describes the radiative transfer of incident photons interacting with canopies bounded underneath by a non-reflecting (‘ black’) surface in a simple way. Incident photons coming though the top of a canopy will either go through the canopy via gaps or interact with canopy leaves (or needles) and other components (e.g., stem and soil). We focus on foliage components here.

The portion of the incident photons that interact with the canopy is defined as canopy interceptance (i_0) (Knyazikhin et al., 2013; Schull et al., 2007; Smolander and Stenberg, 2005). As a result of an interaction, a photon can either be scattered or absorbed by a leaf, depending on the leaf albedo and the wavelength (or frequency) of the photon. Scattered photons may interact with leaves in the canopy again with a given probability. The probability that a photon, after having survived an interaction (i.e., have not been absorbed) with a canopy element, interacts with the canopy is called the recollision probability (p). The probability that the photon after having survived the interaction escapes the canopy through various directional paths is called escape probability ($1 - p$). Remote sensing normally detects signals from one direction above the upper boundary of a canopy. In order to predict the signals in the direction of viewing, another spectral invariant, called directional escape probability ($\rho(\Omega)$), was introduced (Huang et al., 2007).

Canopy scattering s and absorption a are the outcomes of all the interactions between intercepted photons and the canopy. Both a and s of the canopy at wavelength (λ) can be expressed as the sum of a geometric series (Smolander and Stenberg, 2005) and the final expressions are given by:

$$a(\lambda) = i_0 \frac{1 - \omega(\lambda)}{1 - p\omega(\lambda)} \tag{3}$$

$$s(\lambda) = i_0 \frac{(1 - p)\omega(\lambda)}{1 - p\omega(\lambda)} \tag{4}$$

where the numerators represent the contributions for the first order interactions, and the denominators account for contribution of the higher order interactions. Note that the sum of a and s (Eqs. (3) and (4)) is equal to i_0.

By replacing the escape probability ($1 - p$) in Eq. (4) with the directional escape probability $\rho(\Omega)$, TOC directional R is obtained, as follows:

$$R(\Omega, \lambda) = i_0 \rho(\Omega) \frac{\omega(\lambda)}{1 - p\omega(\lambda)} \tag{5}$$

2.2. Linking far-red SIF scattering with reflectance

The scattering of far-red SIF in the viewing direction (σ_F), expressed as a ratio of TOC SIF and SIF emitted by all photosynthetic apparati in the canopy, includes scattering within the leaves, and from the leaf surfaces to the sensors above the canopy.

First, we parametrized the canopy scattering of far-red SIF from the leaf surfaces to the sensor (σ_{FC}), and next we linked σ_{FC} with TOC R. As is the case with TOC R, far-red σ_{FC} can be expressed by using the spectral invariant theory as well (Liu et al., 2018; Yang and Van der Tol, 2018). A TOC SIF observation includes contributions from: 1) emitted SIF photons from leaves that directly escape via $\rho(\Omega)$; 2) emitted SIF photons that interact with leaves in the canopy again (one order), and then escape and are observed via $p\omega(\lambda)\rho(\Omega)$; and 3) the scattered SIF photons that have a second interaction, and then escape in observation direction via $p^2\omega(\lambda)^2\rho(\Omega)$, etc. The total canopy scattering of SIF is the

sum of the contributions, and is given as a geometric series:

$$\sigma_{FC}(\Omega, \lambda) = \rho(\Omega) + p\omega(\lambda)\rho(\Omega) + p^2\omega(\lambda)^2\rho(\Omega) + ... = \frac{\rho(\Omega)}{1 - p\omega(\lambda)} \quad (6)$$

Comparing Eqs. (5) and (6), we obtain the relationship in the NIR region as:

$$\sigma_{FC}(\Omega, \lambda_{nir}) = \frac{R(\Omega, \lambda_{nir})}{i_0\omega(\lambda_{nir})} \quad (7)$$

Eq. (7) shows the link between far-red SIF canopy scattering and NIR reflectance at the wavelength of the SIF measurement. It is worth noting that the exact match between the wavelength of reflectance and that of σ_{FC} described is not strictly necessary. Since both R and σ_{FC} responses in the NIR region are rather flat (Yang and Van der Tol, 2018), a spectrally broader (e.g., ~ 750–900 nm) range of NIR reflectance (R_{nir}) can be used instead of the reflectance at the exact wavelength (λ_{nir}) of the SIF measurement, facilitating FCVI retrievals.

It is important to note that the relationship in Eq. (7) is only valid for far-red SIF and not for red SIF (approximately from 640 to 700 nm). The reason is the asymmetry of leaf reflectance and transmittance in the red. The spectral invariant theory uses only the sum of reflectance and transmittance ($\rho_l + \tau_l$) as input, but the difference ($\rho_l - \tau_l$) is not negligible in the red region (Van der Tol et al., 2019). The relationship shown in Eq. (7) has been derived by using a more generic approach in Yang and Van der Tol (2018), where an explicit discussion on its validity for red and far-red SIF is provided.

The similarity between radiative transfer of SIF and that for incident light is exhibited at leaf level too (Van der Tol et al., 2019). The scattering of far-red SIF within a leaf σ_{FL} is very likely related to leaf scattering (i.e., NIR leaf albedo, ω_{nir}), however, it depends on the physical distribution of the photosynthetic apparatus in the leaf, leaf optical properties (i.e., structure, pigments and dry matter) and the refractive index (Van der Tol et al., 2019) (also see simulations from a leaf model in Fig. S2 in the Supplementary materials). Liu et al. (2018) found that σ_{FL} was close to unity for far-red SIF and σ_{FC} is close to σ_F. The intuitive understanding is that the absorption effects within leaves are weak in the NIR region. The strong scattering leads to large $\sigma_{FL}(\omega_{nir})$ as well as large ω_{nir}. For simplicity, we approximate σ_{FL} by ω_{nir}, noting that both of them are close to unity. With this approximation, we obtain the scattering of far-red SIF in the viewing direction.

$$\sigma_F(\lambda_{nir}) = \sigma_{FC} \times \sigma_{FL} = \frac{R_{nir}}{i_0} \quad (8)$$

2.3. Linking fAPAR to reflectance

The fraction of absorbed photosynthetically active radiation fAPAR is the fraction of incident solar radiation that is absorbed by vegetation in the spectral range from 400 to 700 nm (McCree, 1981). By this definition, fAPAR can be expressed as:

$$\text{fAPAR} = \frac{\int_{400-700\text{ nm}} a(\lambda)E(\lambda)d\lambda}{\int_{400-700\text{ nm}} E(\lambda)d\lambda} \quad (9)$$

where E is the incident irradiance, a is the absorption of the canopy and λ is the wavelength.

To be able to use TOC reflectance to estimate fAPAR, we first express canopy absorption (a) as a function of reflectance by eliminating ω in Eqs. (3) and (5). From Eq. (3), we obtain: $i_0 - a = i_0\frac{\omega}{1-p\omega}(1-p)$; from Eq. (5), we obtain: $R/\rho(\Omega) = i_0\frac{\omega}{1-p\omega}$; and thus obtain:

$$a(\lambda) = i_0 - \frac{1-p}{\rho(\Omega)}R(\lambda) \quad (10)$$

This equation is equivalent to $a(\lambda) = i_0 - s(\lambda)$, because from Eqs. (4) and (5), we know that the quantity $\frac{1-p}{\rho(\Omega)}R(\lambda)$ equals to the canopy scattering (s). Note that $(1-p)/\rho(\Omega)$ is the ratio of canopy scattering in all directions to the scattering in the viewing direction, of which the latter is the directional reflectance.

Introducing Eq. (10) into Eq. (9) yields

$$\begin{aligned}\text{fAPAR} &= i_0 - \frac{1-p}{\rho(\Omega)}\cdot\frac{\int_{400-700\text{ nm}} R(\lambda)E(\lambda)d\lambda}{\int_{400-700\text{ nm}} E(\lambda)d\lambda} \\ &= i_0 - \frac{1-p}{\rho(\Omega)}\bar{R_{vis}} \\ &= i_0\left(1 - \frac{1-p}{i_0\rho(\Omega)}\bar{R_{vis}}\right)\end{aligned} \quad (11)$$

where $\bar{R_{vis}}$ is the broadband visible reflectance ranging from 400 to 700 nm, which may be approximated by the averaged reflectance over all the visible wavelengths.

In Eq. (11), we have linked fAPAR with TOC reflectance, but three spectral invariants are involved as well. We notice that the quantity $\frac{1-p}{i_0\rho(\Omega)}$ is the inverse of the so called directional area scattering factor (DASF = $\frac{i_0\rho(\Omega)}{1-p}$), which is a parameter that describes reflectance of nonabsorbing canopies, and which is independent of the choice of leaf albedo (Knyazikhin et al., 2013). Using this factor, Eq. (11) can also be written as:

$$\text{fAPAR} = i_0\left[1 - \frac{\bar{R_{vis}}}{\text{DASF}}\right] \quad (12)$$

Knyazikhin et al. (2013) demonstrated that DASF is almost proportional to and can be approximated by NIR reflectance (R_{nir}). The reason can be found in Eq. (5). In the near-infrared region, leaf albedo is close to 1 and thus NIR reflectance approximates $\frac{i_0\rho(\Omega)}{1-p}$ (i.e., DASF). Replacing DASF with R_{nir}, we obtain

$$\text{fAPAR} = i_0\frac{R_{nir} - \bar{R_{vis}}}{R_{nir}} \quad (13)$$

This new fAPAR formulation appears similar to NDVI (i.e., $\frac{R_{nir}-Rvis}{R_{nir}+Rvis}$) in terms of the use of NIR and VIS reflectance, however this formulation differs from NDVI and other vegetation indices since it requires the use of canopy interceptance as an input.

2.4. Reflectance index for the radiative transfer factor

Both far-red σ_F and fAPAR are expressed as a function of canopy directional reflectance and canopy interceptance (i.e., Eqs. (8) and (13), respectively). The radiative transfer factor of far-red SIF, defined as the product of these two terms, is expressed as:

$$\Gamma_{rt} = \text{fAPAR} \times \sigma_F = R_{nir} - \bar{R_{vis}} \quad (14)$$

We find that the radiative transfer factor Γ_{rt} can be approximated by the difference of NIR reflectance and broadband VIS reflectance. Note that the unknown term i_0 is eliminated from this equation. According to Eq. (1), normalizing TOC far-red SIF observations by FCVI and iPAR gives the fluorescence emission efficiency (ϵ_F) of the vegetation canopy, as follows:

$$\epsilon_F = \frac{\pi F_{toc}}{\text{iPAR} \times \text{FCVI}} \quad (15)$$

where the units of F_{toc} and iPAR are mW m^{-2} nm^{-1} sr^{-1} and mW m^{-2}, respectively, and the unit of ϵ_F is nm^{-1}. As noted earlier, this approach assumes equivalent geometry conditions for SIF and the FCVI.

3. Methods and materials

Two independent datasets from a field experiment and from a numerical experiment were used to evaluate the performance of FCVI for estimating the radiative transfer factor Γ_{rt} and for calculating canopy fluorescence emission efficiency ϵ_F.

3.1. Field experiment

3.1.1. Study area and field campaign

The field data used in this study were collected in 2017 at the Optimizing Production inputs for Economic and Environmental Enhancement (OPE3) site at the US Department of Agriculture's (USDA) Agricultural Research Service (USDA-ARS) in Beltsville, MD, USA (39.0306°N 76.8454°W, UTC-5). At OPE3, corn (*Zea mays* L.) is planted annually in predominately loamy and sandy soils, which are rain fed and augmented with optimal nitrogen fertilizer rates. The local climate is warm and temperate, with hot, humid summer growing season, and typically mild winters with occasional freezing.

The field data collection and measurement design are described in Campbell et al. (2019). Field measurements covering the whole growing season in 2017 were used, notably from day-of-year (DOY) 192 to DOY 264 except for the period from DOY 210 to DOY 219 due to relocation of experimental instruments to another field. The field measurements were collected on 62 days of which 33 days were sunny or mostly sunny. Corn has distinct growth phases and we identified three phases during the data collection: Young stage (Yn) from DOY 192 to 209 (July 11–28), Mature stage (M) from DOY 220 to 235 (August 8–22) and Senescent stage (S) from DOY 236 to 264 (August 23–September 21). The identification was based on PhenoCam (2017) records and canopy spectral measurements and leaf photosynthetic measurements (for the details, see Campbell et al., 2019).

3.1.2. Canopy SIF and reflectance measurements

TOC reflectance from 400 nm to 1000 nm, TOC SIF in the O_2-B bands at around 687 nm (F_{687}) and in the O_2-A bands at around 760 nm (F_{760}) were collected using a field spectroscopy system FLoX (FLuorescence boX; JB Hyperspectral Devices UG, Dusseldorf, Germany) fixed on a portable tower. These TOC measurements were collected from approximately 1.5 m above the canopy at nadir, covering a 25° field of view (0.66 m diameter at ground level). FLoX simultaneously collected nadir reflectance and SIF measurements from 07:00 to 20:00 (local time). The key settings (i.e., the interval between measurements and the maximum integration time) and the metadata (e.g., spectrometer temperature, detector temperature and humidity, GPS position and time) were stored and available for sorting and filtering of the data.

The FLoX system mainly consists of a QEPro spectrometer (Ocean Optics, USA) and a FLAME-S spectrometer (Ocean Optics, USA). QEPro measures up-welling radiance using a bare fibre and down-welling irradiance using another fibre connected with a cosine corrector from 650 to 800 nm with a very high spectral resolution (Full Width at Half Maximum, FWHM of 0.3 nm). FLAME-S measures up-welling radiance and down-welling irradiance as well, but from 400 to 900 nm with a lower spectral resolution (FWHM of 1.5 nm). Spectral and radiometric calibration and evaluation of the complete system was conducted before and after the field campaign, by the manufacturer and at Goddard Space Flight Center (NASA/GSFC) using light sources calibrated to radiance traceable to National Institute of Standards and Technology (NIST, USA) standards.

TOC reflectance and iPAR were derived from the FLAME-S measurements. iPAR was computed as the integration of the irradiance spectra over the PAR region (400–700 nm). F_{687} and F_{760} were retrieved from the QEPro measurements by using the spectral fitting method (SFM) (Cogliati et al., 2015). The F_{760} measurements were used to examine the performance of FCVI, since FCVI is dedicated for use with far-red SIF but not with red SIF (see Section 2.2). The dataset was filtered to remove measurements obtained at low solar illumination angles to avoid potential artefacts in the data, leaving high quality screened reflectance and SIF measurements obtained in the period from 09:30 to 16:30, which were used in the analysis.

Table 1
Fraction of photosynthetically active radiation absorbed by the leaves ($fAPAR_{leaf}$) measured on corn under optimal nitrogen level at each phenological growth stage in 2017 at OPE3 USDA/ARC, Beltsville, MD.

Growth stage	Measurement DOY	$fAPR_{leaf}$ Mean	$fAPR_{leaf}$ ± stdev
Young	192	0.92	0.007
	199	0.92	0.010
Mature	221	0.91	0.010
	222	0.90	0.030
Senescent	240	0.82	0.030
	263	0.75	0.050

3.1.3. Leaf spectral measurements

Leaf directional-hemispherical reflectance and transmittance factors (DHRF and DHTF, respectively) were measured on several days during the growing season. The measurements were taken on DOY 192 and DOY 199 when the corn was at the young stage, on DOY 221 and DOY 222 at the mature stage, and on DOY 240 and DOY 263 at the senescent stage (Table 1). Nine leaves were used for measurements on each field day, for both abaxial and adaxial sides of the leaves. The spectra in the range from 350 to 2500 nm were measured by using the ASD FieldSpec 4 spectrometer (Malvern Panalytical, Longmont, CO). We used the ASD halogen light source supplied with the integrating sphere in the laboratory. The averaged absorptance (i.e., 1-reflectance-transmittance) of the nine leaves on each day including both abaxial and adaxial measurements were used to estimate $fAPAR_{leaf}$, which is reported in Table 1. $fAPAR_{leaf}$ on the rest of the days was linearly interpolated from those measurements.

3.1.4. Leaf fluorescence measurements

Leaf-level fluorescence was measured *in situ* using an automated MoniPAM fluorometer system (Heinz Walz GmbH, Effeltrich, Germany). The fluorometer collected continuous measurements every 10 min during the day and night. The MoniPAM emitter-detector probes were mounted on fully developed leaves on DOY 190 when canopy closure was approximately 85%. Measurements were collected during the growing season, continuously re-locating the probes, as new leaves emerged. Five emitter-detector probes were operated in parallel using a MoniPAM Data Acquisition system (MONI-DA, Heinz Walz GmbH, Effeltrich, Germany) to measure light-adapted steady state fluorescence (F_s) (Porcar-Castell et al., 2008), which is a broadband measurement of chlorophyll fluorescence in the 710–800 nm range. Three probes were positioned to measure fully sunlit leaves from the upper canopy, while the remaining two probes collected measurements on shaded leaves at varying illumination levels and positions in the canopy. Besides F_s, the PAM measurements included the maximal fluorescence emission level (F_m), the electron transport rate (ETR) and the operating efficiency (YII or ϵ_P) of photosynthesis II (PSII).

Because PAM F_s is the fluorescence signal excited by a constant measuring light intensity and spectral quality, it is regarded as relative fluorescence emission efficiency provided that $fAPAR_{leaf}$ remains the same (Baker, 2008; Schreiber, 1998; Schreiber et al., 1986). However, $fAPAR_{leaf}$ changed during the growing season. To correct for different $fAPAR_{leaf}$ in the growing season and obtain relative leaf ϵ_F, we normalized the measured F_s by $fAPAR_{leaf}$ obtained from the leaf spectral measurements.

3.1.5. Calculation and evaluation of canopy FCVI

Canopy FCVI was computed from the FLAME-S canopy spectral measurements and further used for estimating canopy ϵ_F. For the calculation of FCVI, broadband VIS reflectance ($\bar{R}_{vis}$) was computed as the ratio of the integrated reflected radiation to the integrated incident radiation over the range from 400 to 700 nm. Reflectance at 770 nm was used as R_{nir} for computing FCVI rather than reflectance at 760 nm,

as apparent reflectance at 760 nm is strongly enhanced by SIF contributions (Sabater et al., 2018). FCVI was then computed according to Eq. (14). Canopy ϵ_F was computed as the ratio of F_{760} and the product of FCVI and measured iPAR, according to Eq. (15).

We compared averaged leaf-level ϵ_F measurements from the three MoniPAM heads at upper canopy with the canopy estimated ϵ_F across the growing season, excluding rainy and dense cloudy days as the quality of canopy spectral measurements was not guaranteed under such weather conditions. The leaf-level ϵ_F measurements from the two heads at lower canopy were not used, because the leaf signal available for remote sensing of the canopy is primarily associated with upper canopy and the leaves at lower canopy provided only a small contribution to TOC signals of fully covered canopies. Considering that for consistent interpretation of leaf-level F_s measurements, the ambient light should be stable during the measurement period (Murchie and Lawson, 2013), the midday (12: 00–14:00) F_s measurements, collected under saturating PAR levels for photosynthesis, were used for comparison with the newly derived estimate of ϵ_F.

3.2. Numerical experiment

In the numerical experiment, a dataset consisting of TOC reflectance, far-red SIF and canopy ' true' fluorescence emission efficiency was generated by using the SCOPE model (version 1.70). To include a wide range of practically possible scenarios, we generated 20,736 canopy scenarios. The input of SCOPE for these scenarios comprised 4 chlorophyll content levels, 12 combinations of canopy structure parameters, 3 sun zenith angles, 4 viewing zenith angles, 4 incident radiation levels, 3 levels of air temperature, 3 levels of maximum rate of carboxylation (Table 2). The values of parameters for leaf properties, canopy structure and sun position were chosen within the recommended ranges in SCOPE (Van der Tol et al., 2009; Yang et al., 2017b). A non-reflecting surface was assumed in these scenarios by setting soil reflectance to zero in SCOPE. The usage of non-reflecting surface conformed to the assumption in the theoretical derivation. These scenarios formed the first group.

To examine the soil effects on the performance of FCVI, a second group of simulations was conducted. The scenarios in the second group differed from the first group of scenarios only by soil background. Three subsets of scenarios had different soil backgrounds, while each subset contained 20,736 scenarios covering all possible combinations in Table 2, i.e. as in the first group. Therefore, FCVI was tested for a total of 62,208 scenarios in the second group. Three different soil reflectance spectra were used, including reflectance of a wet soil surface and two brighter and dry soil surfaces (for the reflectance spectra, see Fig. S1 in the Supplementary materials).

We then simulated TOC SIF and TOC reflectance for each scenario. FCVI and iPAR were computed directly from the simulated TOC reflectance and from the incident irradiance spectra, respectively, the same way as computed in the field experiment. Fluorescence emission efficiency ($\epsilon_{F,FCV\ I}$) of all the scenarios was obtained by normalizing the simulated F_{760} by the product of FCVI and iPAR.

The main reason to use SCOPE is that the model serves as the provider of the ' true' values or reference values of ϵ_F. SCOPE simulates total emitted SIF (F_{tot}) by all the leaves in vegetation canopies and APAR (or fAPAR), which allows the calculation of ' true' ϵ_F of the vegetation canopies as follows:

$$\epsilon_{F,SCOPE} = \frac{F_{tot}}{\text{fAPAR} \times \text{iPAR}} \tag{16}$$

The estimated efficiency $\epsilon_{F,FCV\ I}$ at 760 nm using the FCVI approach was compared with the efficiency from the model $\epsilon_{F,SCOPE}$ at 760 nm.

Table 2
Summary of SCOPE inputs applied for the generation of the database.

Parameter	Explanation	Unit	Values
C_{ab}	Chlorophyll a + b content	μg cm^{-2}	10, 20, 40 or 80
LAI	Leaf area index	m^2 m^{-2}	0.5, 1, 3 or 6
LAD	Leaf angle distribution	–	Spherical, planophile, or erectophile
θ_s	sun zenith angle	degree	30, 45 or 60
θ_o	viewing zenith angle	degree	0, 20, 40 or 60
R_{in}	short wave incoming radiation	W m^{-2}	100, 300, 500 or 800
T_{air}	Air temperature	℃	15, 25 or 35
$V_{c\,max}$	The maximum rate of carboxylation	μmol m^{-2} s^{-1}	30, 100 or 160

4. Results

We present results for the field study in Section 4.1 and those from the modelling simulations in Section 4.2.

4.1. Results of the field experiment

Since FCVI is an estimate of fAPAR × σ_F, we expect F_{760} to be related to iPAR × FCVI, and FCVI to be related to the F_{760}/iPAR ratio (Eq. (1)). In Figs. 1 and 2, the results of diurnal and seasonal variations of the two pairs of parameters are presented. In Figs. 3 and 4, the comparison of each pair of parameters is presented. According to the theoretical derivation, the new πF_{760}/iPAR/FCVI variable is an estimate of canopy ϵ_F. In Figs. 5, 6 and 7, the validation of the estimated canopy ϵ_F is presented by comparing with leaf relative ϵ_F measured by the MoniPAM.

4.1.1. Diurnal and seasonal patterns of SIF, iPAR × FCVI, FCVI and SIF/iPAR ratio

The diurnal pattern of F_{760} was similar to that of iPAR × FCVI (Fig. 1a and c). In general, both of them changed diurnally correspondingly to incident radiation (see Fig. S3 in the Supplementary materials), increasing throughout the morning to midday maxima which displayed small dips between 12:00 and 13:00, then declining in the afternoon to values similar to those acquired at the start of the morning. The diurnal patterns of the F_{760}/iPAR ratio and the FCVI were

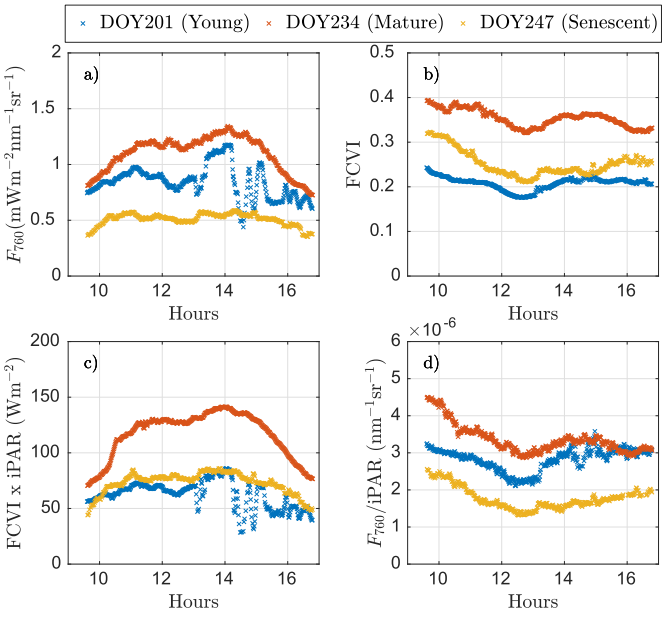

Fig. 1. Diurnal variations of canopy far-red SIF (F_{760}) (a), FCVI (b), FCVI × iPAR (c) and F_{760}/iPAR ratio (d) on one sunny day representative for each growth stage.

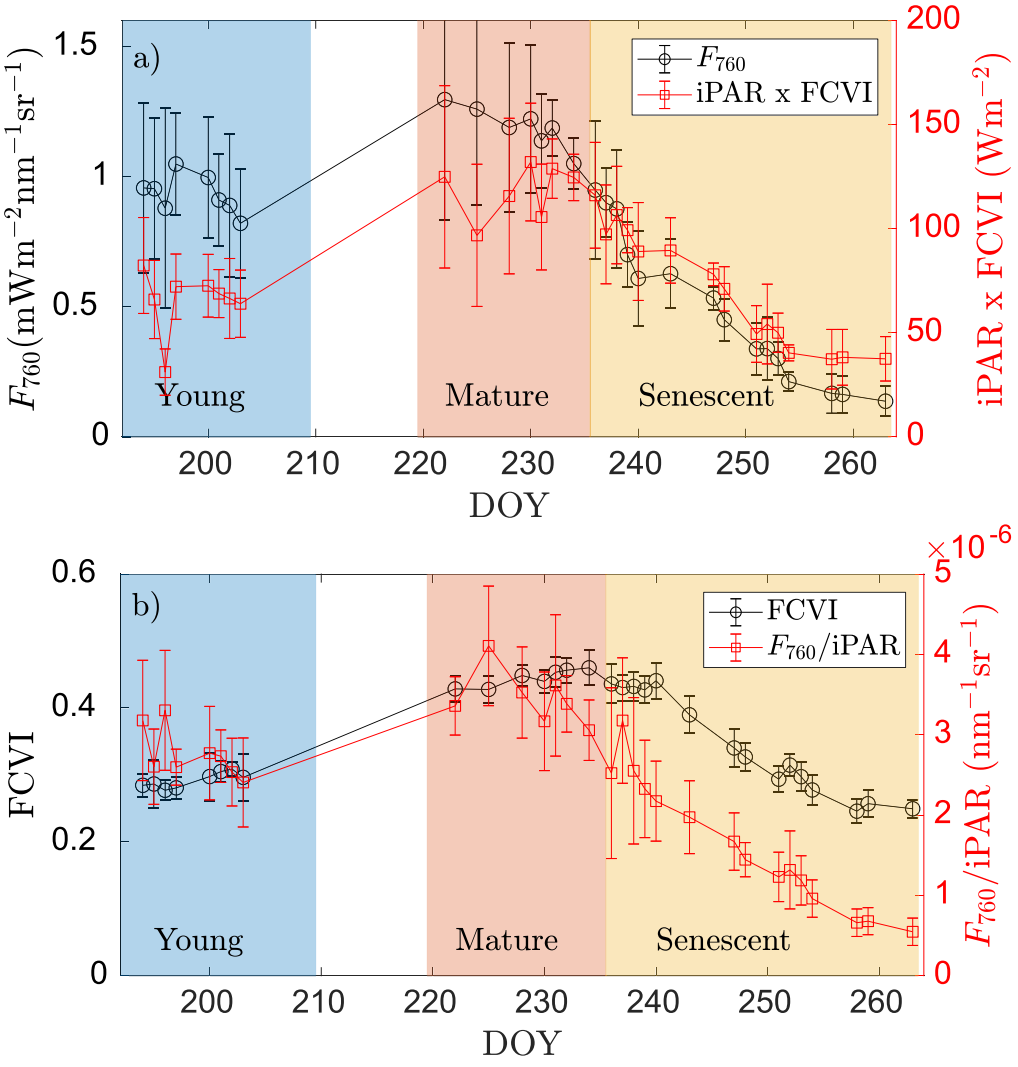

Fig. 2. Seasonal variation of far-red SIF F_{760} (a, left y-axis) and iPAR × FCVI (a, right y-axis), as well as the FCVI (b, left y-axis) and the F_{760}/iPAR ratio (b, right y-axis). Each point represents a daily mean value, and error bar represents ± stdev of measurements.

similar to each other too, and they also displayed midday dips between 12:00 and 13:00 (Fig. 1b and d). However, the relative order (highest to lowest) of those diurnal patterns significantly differed from the diurnal patterns of F_{760} and iPAR × FCVI. While the magnitudes of F_{760} and iPAR × FCVI were significantly lower in the morning than at midday, the magnitudes of FCVI and the F_{760}/iPAR ratio were higher in the morning and decreased throughout the morning to midday after which both increased in the afternoon until 15:30. On DOY 257, the increase in the afternoon lasted until 17:00, while on DOYs 201 and 234, the increase was followed by a decrease. While the FCVI was lowest on DOY 201 at the young stage, the F_{760}/iPAR ratio was lowest on DOY 247 at the senescent stage. While the iPAR × FCVI magnitudes were similar on DOY 201 and 247, F_{760} was much higher on DOY 201 than on DOY 247.

The seasonal patterns of F_{760} and iPAR × FCVI as well as those for the FCVI and the F_{760}/iPAR ratio were similar (Fig. 2). All of these four variables increased from the young to mature stages and then decreased throughout the senescent stage. The agreement within pairs was most evident for F_{760} and iPAR × FCVI (Fig. 2a) late in the growing season, beginning near the transition from mature to senescent canopy. In contrast, the agreement achieved by the other pair (FCVI and F_{760}/iPAR ratio, Fig. 2b) occurred early and late in the observed growth period. Nevertheless, there were other seasonal differences captured in each pair. While F_{760} was significantly higher at the young compared to the senescent stages, the magnitudes of iPAR × FCVI were similar at these two stages. The largest within-pair difference occurred during senescence when the F_{760}/iPAR ratio decreased more dramatically than FCVI. These seasonal pattern differences can also be observed in Fig. 1.

4.1.2. Comparison of SIF and iPAR × FCVI, and comparison of FCVI and SIF/iPAR ratio

We further quantitatively compared all F_{760} measurements with the iPAR × FCVI and this relationship was benchmarked against the commonly utilized relationship between F_{760} and iPAR (Fig. 3). We found that iPAR accounted for only 58% of the observed variation across all F_{760} measurements and 82% for the mid-season mature crop (Fig. 3a). Note that all the correlations reported in this study were statistically significant with $p \leq 0.005$. At the young and the mature stages, the variation in F_{760} of the corn canopy was mainly due to variation in iPAR with $R^2 > 0.70$, while at the senescent stage, iPAR only explained 37% of the variation in F_{760}. Our new iPAR × FCVI term was much more strongly related to F_{760} ($R^2 = 0.91$ overall) than iPAR alone. When using iPAR × FCVI, the overall association with F_{760} increased by 33% across the growing season (Fig. 3b). The mature mid-season crop was described equally well with the two approaches (Fig. 3a and b), whereas the developing and senescent crop stages strongly benefited from the use of FCVI. Particularly at the senescent stage, the inclusion of FCVI (as iPAR × FCVI) resulted in considerably

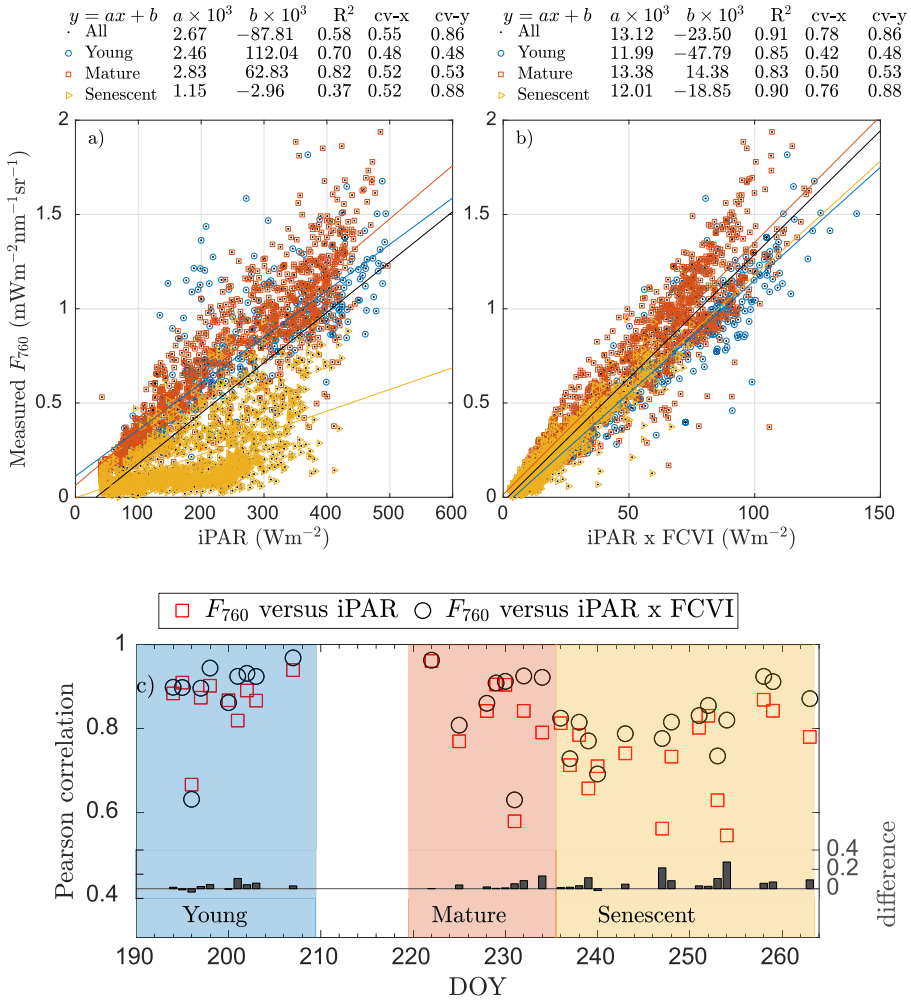

Fig. 3. Comparison of the relationship between measured far-red SIF (F_{760}) versus iPAR (a) and iPAR × FCVI (b), for the corn canopy across the growing season, using diurnal observations at a temporal resolution of 10 min. Note: CV = stdev/mean. Pearson correlation coefficients between F_{760} and iPAR, and coefficients between F_{760} and iPAR × FCVI on individual days and the difference of the coefficients (c).

higher correlation with F_{760} than iPAR, with an increase of R^2 from 0.37 to 0.90. The product iPAR × FCVI displayed the most variation during the senescent stage among the three growth stages, while iPAR had similar variation in each growth stage, as indicated by the coefficients of variation (CVs, the ratio between standard deviation and the mean value). The CVs of F_{760} and iPAR × FCVI in Fig. 3b were ~40% higher for the senescent canopy than for the young and mature canopies.

The strength of the correlations of iPAR × FCVI and F_{760} for most individual measurement days was higher than that of iPAR and F_{760} except for two days in the young stage and one day in the senescent stage. The higher correlations of iPAR × FCVI and F_{760} were most evident for the senescent stage (Fig. 3c), as captured with the Pearson correlation coefficients (r). The diurnal patterns of iPAR × FCVI and F_{760} were similar to each other. This is expressed with the r values obtained between iPAR × FCVI and F_{760}, which were always greater than 0.5 and on 90% of the days, $r > 0.7$.

We also compared all F_{760}/iPAR ratio values with the FCVI (Fig. 4a) and found that the FCVI accounted for 81% of the overall measurement variation. FCVI explained 55% and 70% of the observed variation in the F_{760}/iPAR ratio for the young and senescent stages. However, for the mature stage, when the FCVI had the lowest variation (i.e., CV = 0.11), the FCVI only explained 25% of the variation in the ratio. On individual days, the FCVI and F_{760}/iPAR ratio were also correlated (Fig. 4b). On over 65% of the days, the Pearson correlation coefficient (r) was above 0.6.

4.1.3. Comparisons between leaf and canopy fluorescence emission efficiency

The seasonal patterns of leaf and canopy ϵ_F were similar, both exhibiting significantly lower values at the senescent stage than at the young and mature stages (Fig. 5). Large seasonal variations were found in both leaf and canopy ϵ_F, with magnitudes of ϵ_F at the young stage more than twice those at the senescent stage. However, some differences between leaf and canopy ϵ_F were noticed (Fig. 5). For example, on DOY 229 leaf ϵ_F peaked while canopy ϵ_F clearly did not; also leaf ϵ_F increased between DOY 234 and DOY 236, while canopy ϵ_F decreased slightly. In contrast to the seasonal patterns of leaf and canopy ϵ_F, the first order approximation of efficiency, the F_{760}/iPAR ratio, was seasonally highest at the mature stage, and decreased more dramatically at the senescent stage than either leaf or canopy ϵ_F (see Fig. S4 in the Supplementary materials).

Leaf and canopy ϵ_F were correlated with overall $R^2 = 0.70$, which was much higher than the correlation between leaf ϵ_F and the F_{760}/iPAR ratio ($R^2 = 0.47$) (Fig. 6). Leaf and canopy ϵ_F were strongly correlated at the senescent stage and moderately correlated at the young and mature stages. At mature and senescent stages, both the estimated ϵ_F and the F_{760}/iPAR ratio correlated with leaf ϵ_F comparably well.

In contrast to the seasonal variation, both the estimated canopy ϵ_F and measured leaf ϵ_F had small variations within a day. The coefficients of variation (CV) ranged similarly from 5% to 40% and from 8% to 35% for leaf and canopy ϵ_F, respectively. On over 65% of the days, CVs were

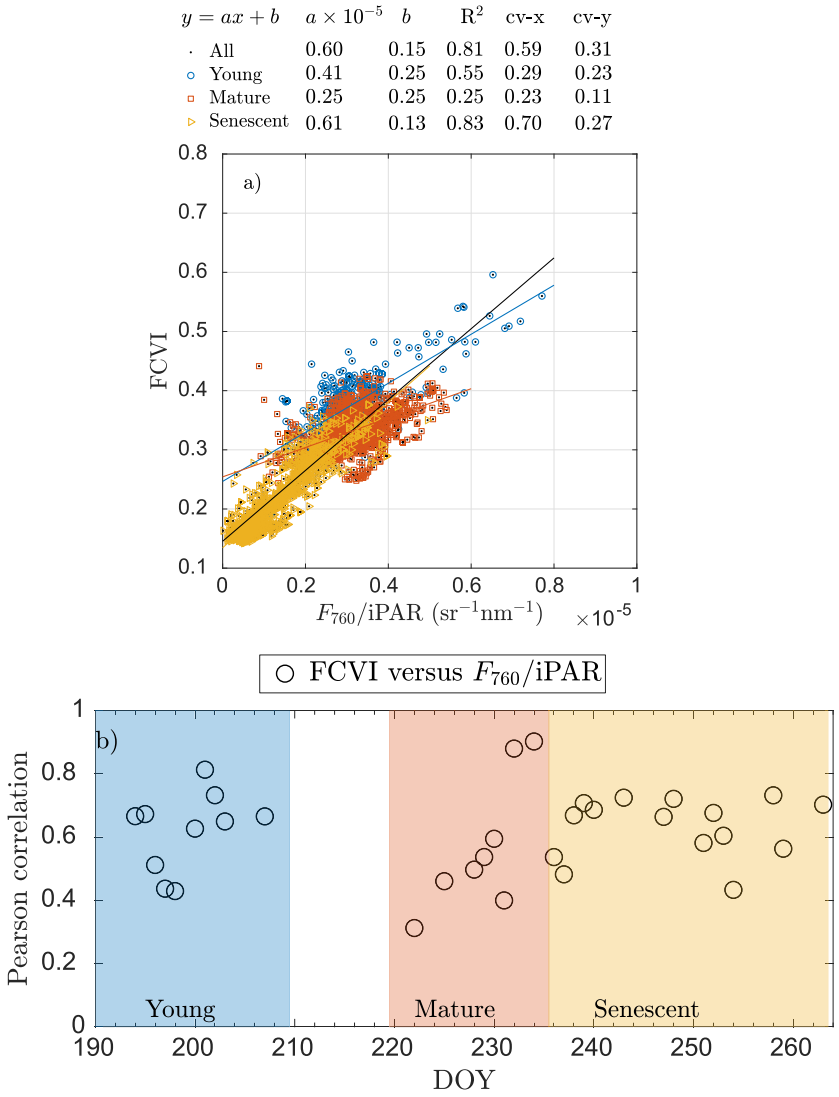

Fig. 4. Comparison of the relationship between measured F_{760}/iPAR ratio versus FCVI for the corn canopy across the 2017 growing season, using diurnal observations at a temporal resolution of 10 min. Note: CV = stdev/mean. Pearson correlation coefficient between FCVI and F_{760}/iPAR ratio on individual days (b).

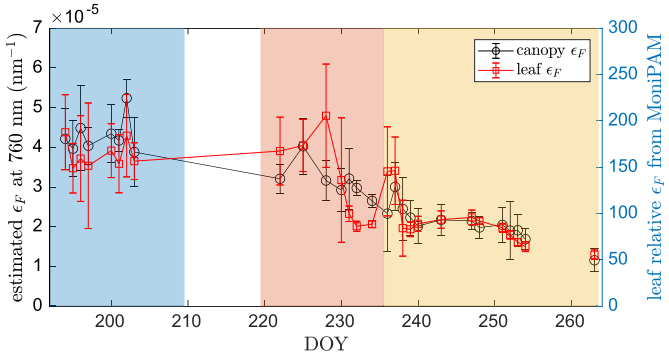

Fig. 5. Comparison between estimated canopy fluorescence emission efficiency from TOC reflectance and SIF measurements and leaf relative fluorescence emission efficiency measured by MoniPAM at middays on sunny or partly cloudy days in the growing season.

less than 25% for both leaf and canopy ϵ_F (data not shown). For example, the estimated canopy ϵ_F changed during each day with variation of less than 30% (Fig. 7b). Similarly to canopy ϵ_F, the variations in leaf relative ϵ_F determined from the MoniPAM within each day were also small. These variations were less than 35% and the largest variation occurred on DOY 201 on which there were clear fluctuations in weather conditions in the afternoon. The correlation between (diurnal) leaf and canopy ϵ_F varied from day to day with r from − 0.7 to 0.88, and on about 50% of the days r ranged from − 0.5 to 0.5 (see Fig. S5 in the Supplementary materials). For example, on the three days presented in Fig. 7, R was 0 (DOY 201), 0 (DOY 234) and 0.45 (DOY 247).

4.2. Results of the numerical experiment

Fig. 8a shows the comparison between the estimated ϵ_F from SIF with FCVI and the SCOPE (i.e., ' true') ϵ_F. We used a non-reflecting soil in the 20736 scenarios in the first group, for which the FCVI successfully estimated the canopy fluorescence emission efficiency from TOC SIF. The correlation between the estimated ϵ_F and the ' true' ϵ_F was very high ($R^2 = 0.92$ and RMSE $= 1.9 \times 10^{-6}$). The relative error of using FCVI to estimate ϵ_F of the 20,736 scenarios, computed as $\frac{\epsilon_{F,FCVI} - \epsilon_{F,SCOPE}}{\epsilon_{F,SCOPE}} \times 100\%$, ranged from − 12% to 18% (Fig. 8c), overestimating ϵ_F at small FCVI and underestimating ϵ_F at high FCVI.

The FCVI performed less well among the 62,208 scenarios bounded underneath by the ' real' soils than for the non-reflecting soil scenarios (Fig. 8b). The relative error ranged from − 62% to 21% and the largest errors occurred for underestimates made at small FCVI values (Fig. 8d), which indicate a small difference between NIR and VIS reflectance. The

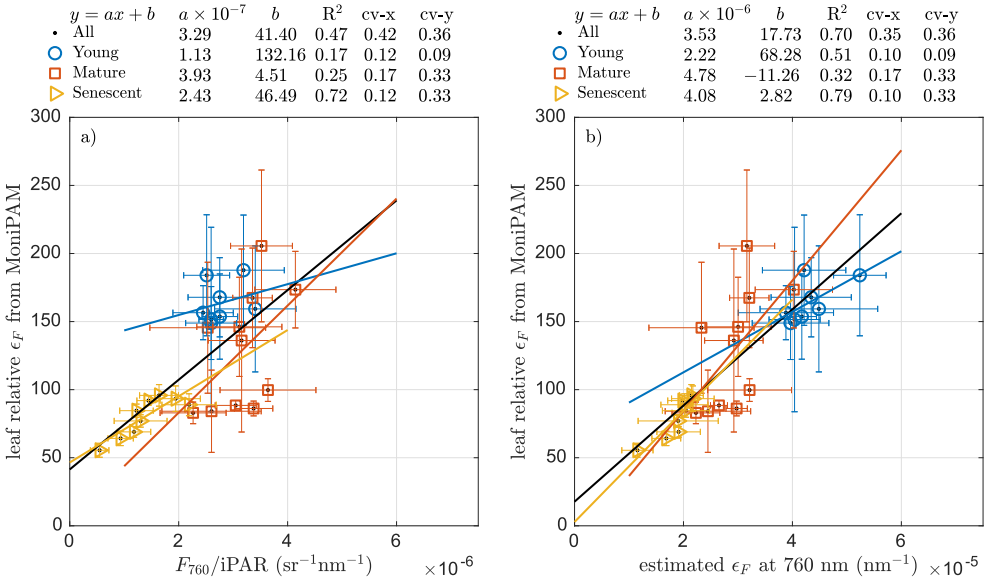

Fig. 6. Comparison of the relationships between leaf relative fluorescence emission efficiency (ϵ_F) versus the F_{760}/iPAR ratio (a) and the estimated fluorescence emission efficiency ($\epsilon_F = \pi F_{760}$/FCVI/iPAR) (b) for the corn canopy at middays on sunny or mostly sunny days across the growing season. Each point represents a daily mean value, and error bar represents ± stdev of measurements. Note: CV = stdev/mean.

relative error followed an exponential function ($y = -140\exp(-12.4x) + 12$) of FCVI with $R^2 = 0.68$. After filtering out the scenarios where the FCVI < 0.18, $\epsilon_{F,FCV\ I}$ and $\epsilon_{F,SCOPE}$ were very close to each other with $R^2 = 0.88$, and their differences were less than 30%. We note that more than 80% of the scenarios we examined had FCVI values greater than 0.18. All FCVI values from scenarios with spherical or planophile leaf angle distribution and LAI ≥ 1 exceeded 0.18. Additionally, we found that when the parameters affecting optical scattering (i.e., LAI and sun angles) were kept constant but photosynthetic functioning related parameters (i.e., $V_{c\,max}$, leaf temperature and incoming radiation) varied, $\epsilon_{F,FCV\ I}$ and $\epsilon_{F,SCOPE}$ appeared to be strongly correlated (see Fig. S6 in the Supplementary materials).

A local sensitivity analysis of FCVI was conducted to illustrate the connection between FCVI and its controlling physical factors. We found that FCVI was very sensitive to LAI, the average leaf inclination angle (ALIA) and viewing zenith angle (Fig. 9). FCVI increased with LAI and decreased with ALIA, such that planophile canopies had the highest FCVI and erectophile canopies the lowest. FCVI increased linearly with θ_o while FCVI was insensitive to θ_s for spherical canopies with LAI = 3. FCVI increased with C_{ab} changing from 10 to 40 μg cm^{-2} but decreased with C_{ab} increasing from 40 to 80 μg cm^{-2}.

5. Discussion

5.1. FCVI for non-physiological components of far-red SIF observations

FCVI quantifies the combined effects of fAPAR and σ_F on far-red SIF, such that the physiologically related variation in SIF can be separated from the non-physiologically variation. This non-physiological contribution is due to leaf optical properties (which affect mostly $R_{\overline{vis}}$), and canopy structure and sun-observer geometry (which affect mostly R_{nir}).

5.1.1. Rationale for using FCVI for non-physiological components

The relations between fAPAR and reflectance and between σ_F and reflectance share a physical basis. The basis of using reflectance to estimate fAPAR is that canopy reflection is complementary to canopy and soil absorption (Smolander and Stenberg, 2005). The basis of using reflectance to estimate σ_F is that the radiative transfer process is totally indifferent to the source of radiation, i.e. whether this was a scattering or an emission event (Yang and Van der Tol, 2018). Both relationships are affected by canopy interceptance: A quantity that is difficult to obtain from remotely sensed signals. The requirement of knowing the value of canopy interceptance in Eqs. (13) and (8) limits their applicability in estimating fAPAR and σ_F separately (Liu et al., 2018; Zeng et al., 2019), but in their product, canopy interceptance is eliminated

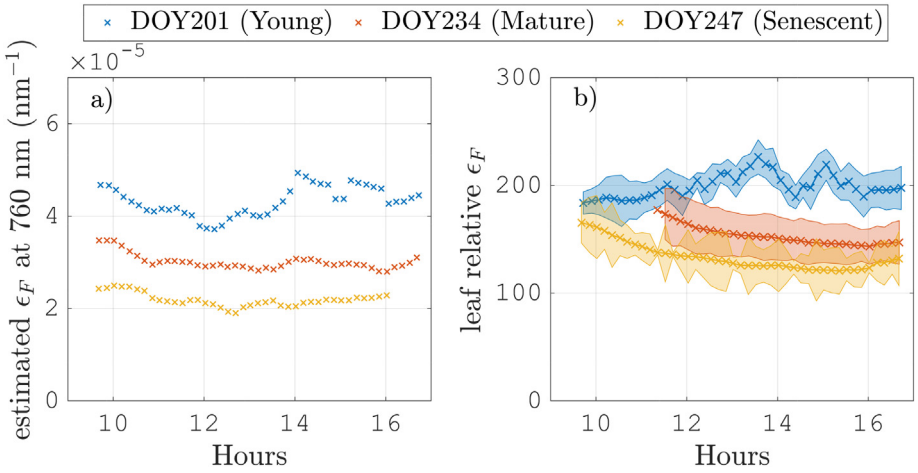

Fig. 7. Diurnal pattern of the estimated fluorescence emission efficiency (a, $\epsilon_F = F_{760}$/iPAR/FCVI) and leaf relative fluorescence emission efficiency (F_s, b) on one representative sunny day for each growth stage. Each point and filled area in b) represent a mean value and ± stdev of measurements of three leaves, respectively.

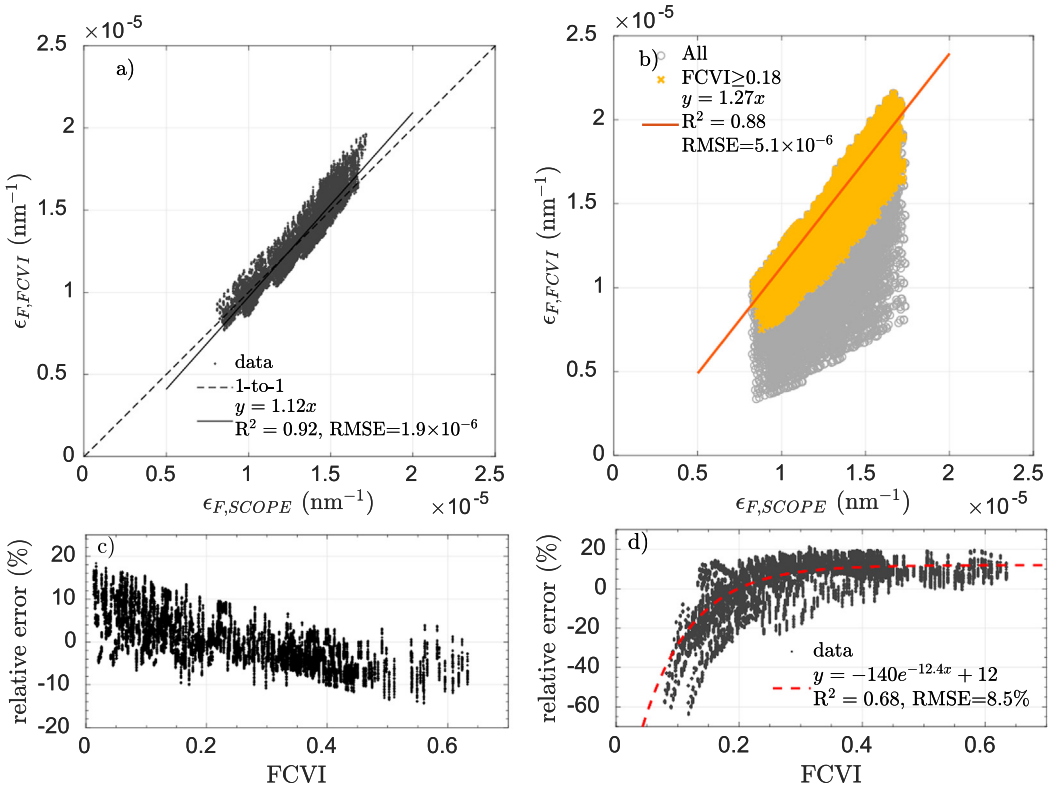

Fig. 8. Comparison between fluorescence emission efficiency used in SCOPE ($\epsilon_{F,SCOPE}$) and estimated fluorescence emission efficiency ($\epsilon_{F,FCV\ I}$) from top-of-canopy reflectance and SIF measurements of the synthetic scenarios in Table 2 bounded underneath by a non-reflecting black soil (a) and non-black (realistic) soils (b), respectively. The relative error of using FCVI to estimate ϵ_F of black soil scenarios (c) and of real soil scenarios (d). Each point represents one scenario.

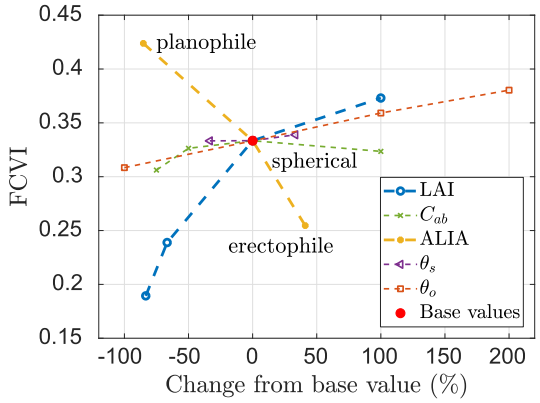

Fig. 9. Spider plot for local sensitivity analysis of FCVI to LAI, leaf chlorophyll C_{ab}, average leaf inclination angles (ALIA), sun zenith angles θ_s and viewing zenith angles θ_o. The base values were set as follows. LAI = 3. C_{ab} = 40 μg cm^{-2}. θ_s = 45°. θ_o = 20°. The base value of ALIA = 57.6° represents a spherical leaf angle distribution.

(Eq. (14)). Thus, we can correct TOC SIF for the combined effects of PAR absorption and SIF scattering without knowing the canopy interception, simply by using FCVI, thus enabling us to obtain physiological information. It is worth noting that visible reflectance is sensitive to the variation in leaf biochemical and biophysical properties and improves the estimation of ϵ_F (see Fig. S7 in the Supplementary materials), although R_{nir} is the dominating factor of FCVI.

Badgley et al. (2017) reported that the simple reflectance index NIRv, which is expressed as R_{nir} ×NDVI (i.e., $R_{nir}\frac{R_{nir}-R_{red}}{R_{nir}+R_{red}}$), also appeared to strongly correlate with SIF through surface vegetated fraction. The idea of NIRv is similar to FCVI, in the sense that NIRv combines the light absorption estimated by NDVI with scattering estimated by R_{nir}. The form of NIRv is also somewhat similar to FCVI: We can write NIRv as $(R_{nir} - R_{red})/(1 + \frac{R_{red}}{R_{nir}})$, where the denominator is close to unity, which in practice does not differ greatly from $R_{nir} - R_{vis}^{-}$. The difference between our approach and NIRv is that FCVI is derived based on the radiative transfer theory with few assumptions and simplifications, while NIRv is semi-empirical. FCVI has a similar form of the difference vegetation index (DVI, $R_{nir} - R_{red}$) (Tucker, 1979). The difference between DVI and FCVI is that broadband visible reflectance is used in FCVI while red reflectance is used in DVI. Moreover, FCVI is dedicated to account for the product of fAPAR and σ_F for far-red SIF while DVI is an indicator of ' greenness' of canopies, which is similar to the function of NDVI (Wiegand, 1977).

In practice, simultaneous measurements of VIS and NIR reflectance and far-red SIF currently are available from many SIF measurement systems, e.g., the HyPlant airborne system (Rascher et al., 2015), field systems such as the FLoX (Campbell et al., 2019), the PhotoSpec (Grossmann et al., 2018) and the FAME (Gu et al., 2019b), as well as from existing satellite missions, e.g., GOME-2 (Joiner et al., 2011), TROPOMI (Guanter et al., 2015) and the upcoming ESA Fluorescence Explorer (FLEX) mission (Drusch et al., 2017).

5.1.2. *Explaining the variation in SIF using FCVI*

FCVI, together with iPAR, can explain most of the variation in SIF observations. We found that both 91% of the variation in all seasonal observations from F_{760} of the corn canopy (Fig. 3a) and a large portion of the variation within individual days (Fig. 3b) were explained by the product of iPAR and FCVI. On the diurnal scale, the variation in TOC SIF of the corn canopy was mainly caused by changes in incoming radiation and sun-observer geometry, which were successfully captured by iPAR and FCVI, respectively. Although the diurnal variation in SIF corresponded closely to the variation in iPAR (Fig. 1a), it was also affected by changes in the sun positions within each day, which led to the diurnal variation of FCVI (Fig. 1b). As a result, iPAR × FCVI was always

better correlated with F_{760} than iPAR alone on each day (Fig. 3). Furthermore, the strong similarity of the diurnal patterns of F_{760} and iPAR × FCVI (Figs. 1a, c and 3b) implies that $\epsilon_F = \frac{F_{760}}{\text{iPAR} \times \text{FCVI}}$ was relatively constant during individual days, which complied with leaf ϵ_F (Fig. 7). On the seasonal scale, the effects of leaf optical properties, canopy structure and sun-observer geometry on TOC SIF were successfully characterized by FCVI as well. The inclusion of FCVI improved the relationship between iPAR and F_{760} at the young and senescent stages (Fig. 3), but at the mature stage when FCVI was relatively stable (Fig. 2a), iPAR × FCVI and iPAR explained the variation in F_{760} equally well (Fig. 3). Nevertheless, the seasonal pattern of iPAR × FCVI and F_{760} had some distinct differences. The inconsistent seasonal patterns of F_{760} and iPAR × FCVI imply that $\epsilon_F = \frac{F_{760}}{\text{iPAR} \times \text{FCVI}}$ varied seasonally, which also complied with leaf ϵ_F (Figs. 5 and 6).

5.2. Deriving physiological information from SIF

5.2.1. Estimating canopy fluorescence light use efficiency

The results from the numerical experiment support the theoretical derivation and expectation that canopy fluorescence emission efficiency (ϵ_F) can be obtained by normalizing TOC far-red SIF by FCVI and iPAR. SCOPE offers a direct validation of this estimated ϵ_F, since the model generates synthetic reference (' true') values of canopy ϵ_F. For canopies bounded underneath by a non-reflecting surface, the error in the estimation of ϵ_F was always less than 30% in a very wide range of scenarios (Fig. 8a). For canopies with reflecting soils this error limit was achieved when FCVI > 0.18 (Fig. 8b), demonstrating the importance of excluding cases with low FCVI which do not provide reliable ϵ_F estimates. In terms of vegetation canopy characteristics, higher values of FCVI indicate higher vegetation coverage and/or LAI, but the exact relation between FCVI and these parameters is affected by sun observer geometry and leaf orientations (Fig. 9). However, we note that SCOPE does not consider variation of leaf optical properties in either vertical or horizontal directions (i.e., 1-D model) and the clumping effects are not considered neither. The model can be used a preliminary validation and more realistic models (e.g., DART and mSCOPE, Yang et al., 2017b) could be used to evaluate the index for complex canopies.

In the field experiment, the estimated canopy ϵ_F of the corn canopy had a similar seasonal pattern to that of the relative leaf ϵ_F (Figs. 5 and 6). The seasonal dynamics of the leaf and canopy ϵ_F were similar to the findings in Goulas et al. (2017) with considerably lower values in the senescent stage. The high correlation between the canopy and leaf ϵ_F on the seasonal scale was consistent with the findings in Cendrero-Mateo et al. (2015), who found that the SIF/iPAR ratio (as a first approximation of canopy ϵ_F) and leaf F_s (as an approximation of leaf ϵ_F) measurements were found to be highly correlated over the growing season across nitrogen treatments. High correlation was also found in the comparison of leaf F_s measurements and canopy SIF/APAR of a temperate forest (Yang et al., 2017a). The SIF/iPAR or SIF/APAR ratios can serve as a surrogate of ϵ_F only if FCVI or σ_F remain stable, respectively, which means leaf optical properties (e.g., chlorophyll content), canopy structure (e.g., LAI) and sun-observer geometry do not significantly change (Fig. 9). For example, for annual crops at the mature stage (Fig. 2a) or evergreen forests, the FCVI is relative stable and thus changes in the SIF/APAR or SIF/iPAR ratios may be interpreted as changes of ϵ_F in this special circumstance.

The seasonal changes in ϵ_F were much larger than the diurnal changes, and the canopy values retrieved from SIF normalized by FCVI and iPAR were consistent with those obtained from F_s as measured for individual leaves with active fluorescence sensors (Figs. 5 and 6). The magnitude of these changes cannot be explained from reversible non-photochemical quenching as modelled by Van der Tol et al. (2014), but it is consistent with earlier reported seasonal changes in F_s attributed to sustained (long term) changes in the partitioning of absorbed energy to non-photochemical quenching processes (Porcar-Castell, 2011).

We also noticed some differences between the leaf and canopy ϵ_F. Canopy ϵ_F is the integral of the leaf efficiencies weighted by the SIF production of each leaf, whereas the efficiencies of individual leaves depend on their exposure to the solar beam, temperature and leaf functional traits such as leaf age and $V_{c\,\max}$. Considering the heterogeneity of the micro-climate in the canopy, a small sample of leaf measurements does not warrant representativeness for the canopy scale. Moreover, by excluding data from high solar zenith angles, we have limited the comparison to the higher end of the irradiance regime, in which diurnal variations in ϵ_F are naturally small (Van der Tol et al., 2014). This may explain the low correlation between leaf and canopy ϵ_F on the diurnal scale.

As a note of caution, we emphasize that even though great care was taken in both the experimental design and the analysis of field data, uncertainties are still present in both leaf and canopy ϵ_F. The canopy ϵ_F was derived from both TOC reflectance and TOC SIF obtained using a state-of-the-art spectrometer and retrieval algorithm. Although we excluded data from unfavourable weather conditions, there is still the need to have independent validations, which require further investigations using different datasets, canopies and species, which are the focus of current efforts by our research team and others. In the field experiment, we have no direct measurements of APAR, which limits investigating the improvement of FCVI in estimating ϵ_F compared with the SIF/APAR ratio (i.e., the effects of σ_F on estimating ϵ_F). In the estimation of the leaf relative ϵ_F, we normalized the MoniPAM F_s measurements by leaf fAPAR measurements, which were available only on several days in the growing season. The linear interpolation approach provided a rough estimation of fAPAR_{leaf} on the other days, but it could have caused some uncertainty in leaf ϵ_F estimations.

5.2.2. Photosynthetic and fluorescence light use efficiency

A possible application of canopy ϵ_F is to improve GPP estimation and to detect crop or forest stress, by exploiting a functional relationship between ϵ_F and ϵ_P. In active fluorescence measurement systems, the difference between leaf steady state and maximal ϵ_F (i.e., when photochemistry is inhibited) provides an accurate estimation of ϵ_P (Genty et al., 1989; Schreiber et al., 1986). In passive SIF observations, clear changes in canopy ϵ_F were observed when the photosynthesis was inhibited by chemical treatment of the vegetation (Celesti et al., 2018; Rossini et al., 2015). However, in conditions where fully inhibited states are not present (which is the default case in the field), we cannot estimate ϵ_P from ϵ_F directly, and we have to be aware that the relationship between steady state ϵ_F and ϵ_P is not unique (Gu et al., 2019a). We found a positive correlation between midday leaf ϵ_P and ϵ_F in the field experiment, but in the literature both positive and negative relationships have been reported. For example, Yang et al. (2017a) reported that the SIF/PAR ratio was positively correlated with leaf ϵ_F and ϵ_P for a temperate forest, while Miao et al. (2018) found that the SIF/APAR ratio was negatively correlated with canopy ϵ_P of a soybean canopy. The strength and even the sign of the relationship depends on irradiance saturation of the photosynthetic apparatus and leaf temperature, which determine the distribution of absorbed photons over photochemical and non-photochemical pathways (Rosema et al., 1998; Van der Tol et al., 2014).

The FCVI may help us understand how ϵ_F varies in different situations using other SIF field studies and appropriate SIF satellite data. This is useful because neither the SIF/PAR nor SIF/APAR ratios used in previous studies directly reveal light use efficiency of fluorescence emission and the reported relationships between ϵ_F and ϵ_P are likely contaminated by leaf optical properties, canopy structure and sun-observer geometry. FCVI accounts for these effects on TOC SIF and makes it possible to retrieve a physiological quantity, ϵ_F, that can be related to ϵ_P or estimates of non-photochemical quenching.

5.3. Limitations of FCVI

5.3.1. Black soil problem

The derivation in Section 2 is based on a black-soil simplification that assumes vegetation canopies are bounded underneath by a non-reflecting surface (i.e., ' black soil'), which is inherited from the spectral invariant theory (Knyazikhin et al., 2011).

The impact of the black-soil assumption on Γ_{rt} can be qualitatively analysed as follows. A reflecting soil enhances both σ_F and fAPAR, and thus Γ_{rt}, compared to a non-reflecting soil. It enhances fAPAR because of canopy absorption of the soil's reflected radiation. The reflecting soil also leads to an increase of σ_F because the emitted SIF photons have the chance to bounce into the viewing direction after hitting the soil background. Therefore, Γ_{rt} of a vegetation canopy is greater when the canopy is bounded underneath by a reflecting soil rather than a non-reflecting soil.

However, the impact of the black-soil assumption on FCVI is unclear. Although the reflecting soil enhances both VIS and NIR reflectance, the magnitudes of the enhancement in the two spectral regions, and thus their difference (i.e., FCVI) depends on soil and canopy spectral characteristics. Soil background alters the relationship between the FCVI and Γ_{rt} for incomplete canopy covers and/or low LAI. As a result, using FCVI as a substitute for Γ_{rt} to estimate ϵ_F of canopies with low vegetation coverage is inaccurate (Fig. 8b). For example, we found that canopies with spherical leaf angle distribution and LAI < 1 had FCVI lower than 0.18 and relative error of using FCVI to estimate ϵ_F of these canopies could be as high as 60%.

Recently, Zeng et al. (2019) proposed a practical approach to account for the soil background effect on far-red SIF scattering (σ_F) by using NDVI. To correct for the soil effect, they proposed to use the NIRv (NIRv $= R_{nir} \times$ NDVI) instead of R_{nir} alone. The NDVI was proposed as a proxy for the contribution of ' pure' vegetation signals, excluding the soil effect on R_{nir}. With this concept, they extended the previous approach presented in Yang and Van der Tol (2018), where $\sigma_F = R_{nir}/i_0$, and estimated σ_F by $R_{nir} \times$ NDVI/i_0. If the effect of the soil on fAPAR is ignored, we can apply a correction of FCVI for non-black soils can be applied by multiplication with NDVI. Alternatively, from Zeng et al. (2019) approach, we can easily obtain an estimation of Γ_{rt} as $R_{nir} \times$ NDVI, which is NIRv proposed in Badgley et al. (2017).

To examine and evaluate the performance of NDVI in accounting for the soil effects on the estimates of σ_F and Γ_{rt}, we repeated the experiment in Zeng et al. (2019). For a reasonable comparability, we used the same scenarios (expressed as the parameters LAI, chlorophyll content, soil reflectance, sun and viewing zenith angles) and the same version of the SCOPE model as used in Zeng et al. (2019). In the evaluation of the performance, we concentrate on the most challenging conditions, notably sparse canopies, and present the scenarios with low LAI (i.e., LAI $= 0.5$ or 1).

For sparse canopies the inclusion of NDVI in the R_{nir}-approach ($\sigma_F = R_{nir} \times$NDVI/$i_0$) resulted in a small improvement in estimated σ_F as compared to the original R_{nir}-based approach ($\sigma_F = R_{nir}/i_0$) (Fig. 10). However, the relative errors of both approach were high ranging from -70 % to 200% for R_{nir}-based approach and -100 % to 70% for the other approach (Fig. 10c). Both approaches could not provide a satisfactory estimation of σ_F for sparse canopies. The approach using NDVI performed slightly better in some scenarios (e.g., LAI $= 0.5$ and erectophile canopies), but the improvement is insufficient if the aim is to estimate Γ_{rt} and retrieve ϵ_F (Fig. 10b). Fig. 10d confirms this. For low values of Γ_{rt}, where the soil contributions are largest, NIRv and FCVI $\times$ NDVI seem to better estimates than FCVI. It could be that NDVI partly accounts the soil effects in these cases. However, the inclusion of NDVI overall weakened the performance of FCVI in predicting Γ_{rt}. The absolute difference between FCVI and Γ_{rt} ranged between 0 and 60%, and in $\sim$ 75% of the simulated scenarios FCVI differed less than 25% from Γ_{rt}. In contrast, FCVI $\times$ NDVI differed from Γ_{rt} by up to 160% and in $\sim$ 75% of the scenarios the difference was more than 50% of Γ_{rt}. The relative errors of using NIRv to predict Γ_{rt} ranged from -55% to 50%.

As discussed in Section 5.1.1, NIRv and FCVI are close to each other. Nevertheless, we emphasize again that the derivation of FCVI follows the radiative transfer theory with few assumptions and simplifications, while the use of NDVI is debatable.

Intuitively, multiplying $\frac{R_{nir}}{i_0}$ or FCVI by NDVI can to some extend correct for the soil effects, since NDVI is highly related to canopy coverage and soil fraction. However, there is no theoretical basis in radiative transfer for using NDVI for this purpose. Zeng et al. (2019) used NDVI as a measure of the contribution of single (i.e., first-order) scattering from the leaves to R_{nir}. The contribution of first-order scattering from leaves depends on the sun and viewing angles and on the leaf scattering phase function, which is determined by the leaf inclination distribution and optical properties (Nilson and Kuusk, 1989). Therefore, it is not justified to assume that the NDVI can account for all of these effects. Furthermore, the use of fAPAR for i_0 in Zeng et al. (2019) is questionable because i_0 only depends on canopy structure and sun position while fAPAR is largely affected by leaf pigment pool (e.g., chlorophyll content). In the numerical experiment of Zeng et al. (2019), only the effects of variation in chlorophyll content are examined and the synthetic scenarios do not cover low chlorophyll content (the content of all the scenarios is ≥ 40 μg cm^{-2}). The applicability of NDVI and the approximation of i_0 by fAPAR still require further investigation.

We were not able to establish a simple correction for multiple soil effects that does not require strong assumptions and that would introduce new uncertainties and reduce the applicability range of the method. For this reason, we recommend the use of filters or masks to exclude canopies with low vegetation coverage, as illustrated in Fig. 8. According to the results from the numerical experiment, FCVI $= 0.18$ is a practical threshold. In the numerical experiment, we have examined a wide range of scenarios and all scenarios with FCVI greater than 0.18 had a relative error less than 30%. Therefore, the threshold appears representative and it is applicable to most field conditions and campaigns. The use of an FCVI threshold is preferred to of a threshold based on LAI or vegetation coverage for two reasons: first FCVI can be directly obtained from remote sensing data with limited processing, and second, an FCVI filter includes the combined effects of sun-observer geometry, LAI, vegetation cover and leaf orientation.

For vegetation with FCVI < 0.18, our approach is not sufficiently accurate for estimation of ϵ_F. For those cases other techniques may be attempted, such as spectral mixture analysis (e.g., Asner and Heidebrecht, 2002, Zeng et al., 2019) to first decompose an image into photosynthetic vegetation and bare soil contributions, after which our approach can be applied to the decomposed pure vegetation FCVI and TOC SIF. Alternatively, full radiative transfer model inversions can be carried out for those pixels, although this is computationally demanding (Yang et al., 2019).

5.3.2. fAPAR by chlorophyll and by the whole canopy

An important issue to consider when using SIF to derive information on vegetation photosynthetic function is the difference between fAPAR_{chl} and fAPAR. FCVI is a good estimate of the product of fAPAR and σ_F, but fAPAR_{chl} is the exact quantity that accounts for the effects of the light absorption process since only the radiation absorbed by chlorophyll can be re-emitted as F_{760}. For green vegetation, APAR is typically used for evaluation of photosynthetic activity, assuming that fAPAR is close to fAPAR_{chl}. In some cases, the absorption by non-photosynthetic components of the canopy, such as cellulose and carotenoids, cannot be neglected. Based on the SCOPE simulations, the ratio of fAPAR and fAPAR_{chl} of the synthetic scenarios in the first group ranged from 1.05 to 1.5 and the ratio was higher in the canopies with lower chlorophyll content. Therefore, relying on fAPAR instead of fAPAR_{chl}, can produce an overestimation of Γ_{rt} and an underestimation of canopy ϵ_F. This might have caused some errors in the estimated ϵ_F of the corn canopy, especially in the senescent stage, when fAPAR

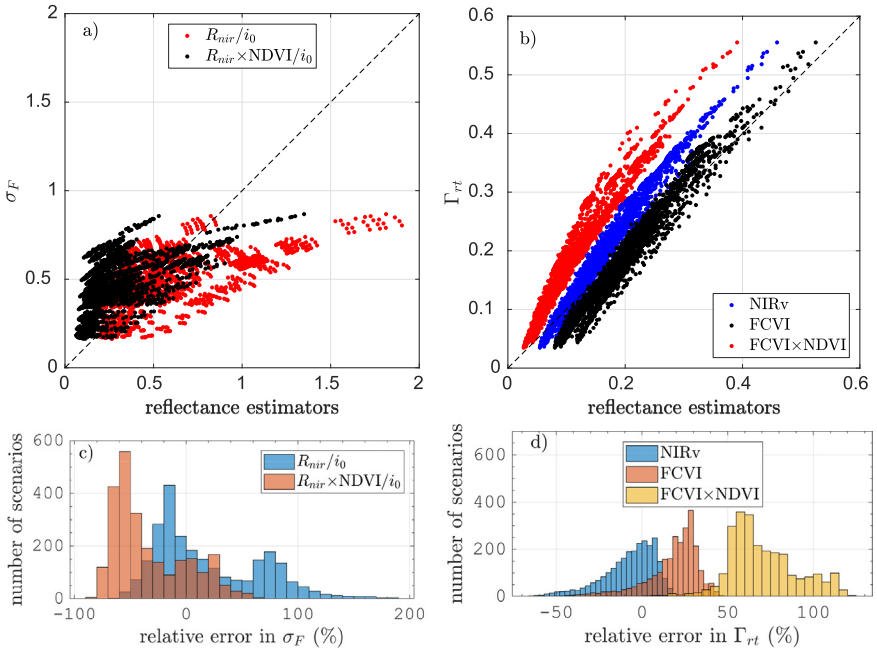

Fig. 10. Comparison of reflectance estimators with σ_F (a, c) and Γ_{rt} (b, d) of synthetic sparse vegetation canopies. The scenarios used here were the same as in Table1 in Zeng et al. (2019).

considerably differs from $fAPAR_{chl}$. This problem will be addressed in a follow-up study. However, we note that $fAPAR_{chl}$ has successfully been retrieved from MODIS and the Earth Observing-1 Hyperion satellite imagery (Middleton et al., 2018; Zhang et al., 2014, 2016) and measured in the field for forests and agriculture (Gitelson, 2019). In a follow-up study of the relationship between measured/estimated fAPAR and $fAPAR_{chl}$, we could perform a correction of FCVI (e.g., using the ratio of MODIS fAPAR and $fAPAR_{chl}$ products) to account for the difference between fAPAR and $fAPAR_{chl}$.

5.3.3. Simplification of leaf optical properties in the spectral invariant theory

The derivation in Section 2 was based on the spectral invariant theory. This theory uses only leaf albedo (ω) to characterize the leaf optical properties (i.e., leaf scattering) and does not differentiate between leaf reflectance (ρ_l) and transmittance (τ_l). However, although radiative transfer is indifferent to the origin of the photons (e.g., scattering or SIF emission), it does depend on the direction of the flux. In the derivation of Eq. (8) it was assumed that the partitioning of the scattered radiation over the two surfaces (i.e., the illuminated and shaded sides) was equal to the partitioning of the emitted fluorescence over the two sides of the leaves (Yang and Van der Tol, 2018). Without this assumption, the relationship between reflectance and SIF is more complicated (Yang and Van der Tol, 2018), an aspect that is not considered in Liu et al. (2018) or Zeng et al. (2019). Field measurements (Van Wittenberghe et al., 2015) and model simulations (Van der Tol et al., 2019) show that this assumption is reasonable in the NIR spectral region, but not in the red region. In the NIR region, this asymmetry problem is likely responsible for the difference between estimated and 'true' σ_F in Fig. 8a.

Although in this study we only examined the commonly used far-red SIF at 760 nm, the FCVI approach for estimating ϵ_F should work at other far-red bands, such as 740 nm and 757 nm (see Fig. S8 in the Supplementary materials). The applicability of FCVI at other bands mainly depends on the partitioning of the scattered radiation over the two surfaces and the partitioning of the emitted fluorescence over the two sides of the leaves. Leaf chlorophyll absorption can cause significant difference between the partitioning of the emitted fluorescence and scattered radiation (Van der Tol et al., 2019; Yang and Van der Tol, 2018). At the chlorophyll absorption bands or close to these bands, the relationship $\sigma_F = R_{nir}/i_0$ does not hold and thus the use of FCVI may not provide a promising estimation of ϵ_F

6. Conclusions

Remote sensing measurements of SIF are controlled by both physiological processes and radiative transfer processes in the vegetation canopy. We have proposed a physically-based reflectance index (FCVI) to quantify simultaneously the leaf biochemical, canopy structure and sun-observer geometry effects on far-red SIF. The index, expressed as the difference between NIR and broadband VIS reflectance, accounts for the effects of photosynthetic light absorption, re-absorption and fluorescence scattering on far-red SIF observations in relatively dense canopies.

FCVI provides an estimate of the effects of PAR absorption and far-red SIF scattering into the viewing direction in moderately dense canopies. Thus, far-red SIF normalized by the product of FCVI and incident PAR quantifies the fluorescence emission efficiency in the far-red region. In the field study, the estimated canopy fluorescence emission efficiency had a similar seasonal pattern to the PAM measured leaf fluorescence emission efficiency. Using the FCVI to estimate the fluorescence emission efficiency has a clear advantage compared to using RTMs because it only requires TOC reflectance and does not depend on the prior information about the vegetation's leaf and canopy parameters. However, for sparse vegetation with FCVI < 0.18 this approach is not accurate enough to estimate far-red fluorescence emission efficiency. The FCVI derivation is useful by itself as a means of providing insight into the canopy radiative transfer processes affecting remote sensing observations of vegetation photosynthesis. The combined use of FCVI and far-red SIF is expected to provide a practical approach for plant physiology monitoring through remote sensing.

CRediT authorship contribution statement

Peiqi Yang: Conceptualization, Methodology, Writing - original draft, Data curation, Visualization, Investigation, Validation, Software, Writing - review & editing. **Christiaan van der Tol:** Conceptualization, Methodology, Supervision, Writing - review & editing. **Petya K.E.**

Campbell: Data curation, Writing - review & editing. **Elizabeth M. Middleton:** Supervision, Writing - review & editing.

Declaration of competing interest

The authors declare that they have no known competing financial interests or personal relationships that could have appeared to influence the work reported in this paper.

Acknowledgments

The work of the first author (Peiqi Yang) was supported by the Netherlands Organization for Scientific Research (NWO) in the frame of the Earth and Life Sciences (ALW) division, project ALWGO.2018.018. The collection of field data and the work of co-authors Campbell and Middleton were supported by NASA's Terrestrial Ecology and Land Cover Land Use Change programs, and the Biospherc-Sciences Laboratory at NASA Goddard Space Flight Center. We express our special thanks to Joanna Joiner and Yasuko Yoshida for constructive comments and suggestions to improve the quality of the manuscript. We also thank the Editor and anonymous reviewers for constructive feedback to improve the quality of our manuscript.

Appendix A. Supplementary data

Supplementary data to this article can be found online at https://doi.org/10.1016/j.rse.2020.111676.

References

Ač, A., Malenovskỳ, Z., Olejníčková, J., Gallé, A., Rascher, U., Mohammed, G., 2015. Meta-analysis assessing potential of steady-state chlorophyll fluorescence for remote sensing detection of plant water, temperature and nitrogen stress. Remote Sens. Environ. 168, 420–436.

Asner, G.P., Heidebrecht, K.B., 2002. Spectral unmixing of vegetation, soil and dry carbon cover in arid regions: comparing multispectral and hyperspectral observations. Int. J. Remote Sens. 23 (19), 3939–3958.

Badgley, G., Field, C.B., Berry, J.A., 2017. Canopy near-infrared reflectance and terrestrial photosynthesis. Sci. Adv. 3 (3), e1602244.

Badgley, G., Anderegg, L.D., Berry, J.A., Field, C.B., 2018. Terrestrial gross primary production: using NIRV to scale from site to globe. Glob. Chang. Biol.

Baker, N.R., 2008. Chlorophyll fluorescence: a probe of photosynthesis in vivo. Annu. Rev. Plant Biol. 59, 89–113.

Campbell, P.K., Huemmrich, K.F., Middleton, E.M., Ward, L.A., Julitta, T., Daughtry, C.S., Burkart, A., Russ, A.L., Kustas, W.P., 2019. Diurnal and seasonal variations in chlorophyll fluorescence associated with photosynthesis at leaf and canopy scales. Remote Sens. 11 (5), 488.

Celesti, M., van der Tol, C., Cogliati, S., Panigada, C., Yang, P., Pinto, F., Rascher, U., Miglietta, F., Colombo, R., Rossini, M., 2018. Exploring the physiological information of sun-induced chlorophyll fluorescence through radiative transfer model inversion. Remote Sens. Environ. 215, 97–108.

Cendrero-Mateo, M.P., Moran, M.S., Papuga, S.A., Thorp, K., Alonso, L., Moreno, J., Ponce-Campos, G., Rascher, U., Wang, G., 2015. Plant chlorophyll fluorescence: active and passive measurements at canopy and leaf scales with different nitrogen treatments. J. Exp. Bot. 67 (1), 275–286.

Cogliati, S., Verhoef, W., Kraft, S., Sabater, N., Alonso, L., Vicent, J., Moreno, J., Drusch, M., Colombo, R., 2015. Retrieval of sun-induced fluorescence using advanced spectral fitting methods. Remote Sens. Environ. 169, 344–357.

Drusch, M., Moreno, J., Del Bello, U., Franco, R., Goulas, Y., Huth, A., Kraft, S., Middleton, E.M., Miglietta, F., Mohammed, G., et al., 2017. The FLuorescence EXplorer Mission Concept-ESA's Earth Explorer 8. IEEE Trans. Geosci. Remote Sens. 55 (3), 1273–1284.

Genty, B., Briantais, J.-M., Baker, N.R., 1989. The relationship between the quantum yield of photosynthetic electron transport and quenching of chlorophyll fluorescence. Biochim. Biophys. Acta Gen. Subj. 990 (1), 87–92.

Gitelson, A.A., 2019. Remote estimation of fraction of radiation absorbed by photosynthetically active vegetation: generic algorithm for maize and soybean. Remote Sens. Lett. 10 (3), 283–291.

Goulas, Y., Fournier, A., Daumard, F., Champagne, S., Ounis, A., Marloie, O., Moya, I., 2017. Gross primary production of a wheat canopy relates stronger to far red than to red solar-induced chlorophyll fluorescence. Remote Sens. 9 (1), 97.

Grossmann, K., Frankenberg, C., Magney, T.S., Hurlock, S.C., Seibt, U., Stutz, J., 2018. PhotoSpec: A new instrument to measure spatially distributed red and far-red solar-induced chlorophyll fluorescence. Remote Sens. Environ. 216, 311–327.

Gu, L., Han, J., Wood, J.D., Chang, C.Y.-Y., Sun, Y., 2019a. Sun-induced Chl fluorescence and its importance for biophysical modeling of photosynthesis based on light reactions. N. Phytol.

Gu, L., Wood, J., Chang, C.-Y., Sun, Y., Riggs, J., 2019b. Advancing terrestrial ecosystem science with a novel automated measurement system for sun-induced chlorophyll fluorescence for integration with eddy covariance flux networks. J. Geophys. Res. Biogeo. 124 (1), 127–146.

Guanter, L., Zhang, Y., Jung, M., Joiner, J., Voigt, M., Berry, J.A., Frankenberg, C., Huete, A.R., Zarco Tejada, P., Lee, J.-E., et al., 2014. Global and time-resolved monitoring of crop photosynthesis with chlorophyll fluorescence. Proc. Natl. Acad. Sci. 111 (14), E1327–E1333.

Guanter, L., Aben, I., Tol, P., Krijger, J., Hollstein, A., Köhler, P., Damm, A., Joiner, J., Frankenberg, C., Landgraf, J., 2015. Potential of the TROPOspheric Monitoring Instrument (TROPOMI) onboard the Sentinel-5 Precursor for the monitoring of terrestrial chlorophyll fluorescence. Atmos. Meas. Tech. 8 (3), 1337–1352.

He, L., Chen, J.M., Liu, J., Mo, G., Joiner, J., 2017. Angular norMalization of GOME-2 sun-induced chlorophyll fluorescence observation as a better proxy of vegetation productivity. Geophys. Res. Lett.

Hernández-Clemente, R., North, P.R., Hornero, A., Zarco-Tejada, P.J., 2017. Assessing the effects of forest health on sun-induced chlorophyll fluorescence using the FluorFLIGHT 3-D radiative transfer model to account for forest structure. Remote Sens. Environ. 193, 165–179.

Huang, D., Knyazikhin, Y., Dickinson, R.E., Rautiainen, M., Stenberg, P., Disney, M., Lewis, P., Cescatti, A., Tian, Y., Verhoef, W., et al., 2007. Canopy spectral invariants for remote sensing and model applications. Remote Sens. Environ. 106 (1), 106–122.

Huete, A., Didan, K., Miura, T., Rodriguez, E.P., Gao, X., Ferreira, L.G., 2002. Overview of the radiometric and biophysical performance of the MODIS vegetation indices. Remote Sens. Environ. 83 (1-2), 195–213.

Joiner, J., Yoshida, Y., Vasilkov, A., Middleton, E., et al., 2011. First observations of global and seasonal terrestrial chlorophyll fluorescence from space. Biogeosciences 8 (3), 637–651.

Knyazikhin, Y., Schull, M.A., Xu, L., Myneni, R.B., Samanta, A., 2011. Canopy spectral invariants. Part 1: a new concept in remote sensing of vegetation. J. Quant. Spectrosc. Radiat. Transf. 112 (4), 727–735.

Knyazikhin, Y., Schull, M.A., Stenberg, P., M ottus, M., Rautiainen, M., Yang, Y., Marshak, A., Carmona, P.L., Kaufmann, R.K., Lewis, P., et al., 2013. Hyperspectral remote sensing of foliar nitrogen content. Proc. Natl. Acad. Sci. 110 (3), E185–E192.

Lewis, P., Disney, M., 2007. Spectral invariants and scattering across multiple scales from within-leaf to canopy. Remote Sens. Environ. 109 (2), 196–206.

Liu, X., Guanter, L., Liu, L., Damm, A., Malenovskỳ, Z., Rascher, U., Peng, D., Du, S., Gastellu-Etchegorry, J.-P., 2018. Downscaling of solar-induced chlorophyll fluorescence from canopy level to photosystem level using a random forest model. Remote Sens. Environ.

Lu, X., Liu, Z., An, S., Miralles, D.G., Maes, W., Liu, Y., Tang, J., 2018. Potential of solar-induced chlorophyll fluorescence to estimate transpiration in a temperate forest. Agr. Forest. Meteorol. 252, 75–87.

Maxwell, K., Johnson, G.N., 2000. Chlorophyll fluorescence — a practical guide. J. Exp. Bot. 51 (345), 659–668.

McCree, K.J., 1981. Photosynthetically active radiation. In: Physiological Plant Ecology I. Springer, pp. 41–55.

Miao, G., Guan, K., Yang, X., Bernacchi, C.J., Berry, J.A., DeLucia, E.H., Wu, J., Moore, C.E., Meacham, K., Cai, Y., et al., 2018. Sun-induced chlorophyll fluorescence, photosynthesis, and light use efficiency of a soybean field from seasonally continuous measurements. J. Geophys. Res. Biogeo. 123 (2), 610–623.

Middleton, E.M., Huemmrich, K.F., Zhang, Q., Campbell, P.K., Landis, D.R., 2018. Photosynthetic Efficiency and Vegetation Stress. Biophysical and Biochemical Characterization and Plant Species Studies. pp. 133.

Migliavacca, M., Perez-Priego, O., Rossini, M., El-Madany, T.S., Moreno, G., van der Tol, C., Rascher, U., Berninger, A., Bessenbacher, V., Burkart, A., et al., 2017. Plant functional traits and canopy structure control the relationship between photosynthetic CO_2 uptake and far-red sun-induced fluorescence in a Mediterranean grassland under different nutrient availability. N. Phytol.

Monteith, J., 1972. Solar radiation and productivity in tropical ecosystems. J. Appl. Ecol. 9 (3), 747–766.

Murchie, E.H., Lawson, T., 2013. Chlorophyll fluorescence analysis: a guide to good practice and understanding some new applications. J. Exp. Bot. 64 (13), 3983–3998.

Myneni, R., Hoffman, S., Knyazikhin, Y., Privette, J., Glassy, J., Tian, Y., Wang, Y., Song, X., Zhang, Y., Smith, G., et al., 2002. Global products of vegetation leaf area and fraction absorbed PAR from year one of MODIS data. Remote Sens. Environ. 83 (1), 214–231.

Nilson, T., Kuusk, A., 1989. A reflectance model for the homogeneous plant canopy and its inversion. Remote Sens. Environ. 27 (2), 157–167.

PhenoCam, 2017. Phenocam — an ecosystem phenology web camera network. https://phenocam.sr.unh.edu/webcam/.

Porcar-Castell, A., 2011. A high-resolution portrait of the annual dynamics of photochemical and non-photochemical quenching in needles of *Pinus sylvestris*. Physiol. Plant. 143 (2), 139–153.

Porcar-Castell, A., Pfündel, E., Korhonen, J.F., Juurola, E., 2008. A new monitoring PAM fluorometer (MONI-PAM) to study the short- and long-term acclimation of photosystem II in field conditions. Photosynth. Res. 96 (2), 173–179.

Porcar Castell, A., Tyystjärvi, E., Atherton, J., van der Tol, C., Flexas, J., Pfündel, E.E., Moreno, J., Frankenberg, C., Berry, J.A., 2014. Linking chlorophyll a fluorescence to photosynthesis for remote sensing applications: mechanisms and challenges. J. Exp. Bot. eru191.

Rascher, U., Alonso, L., Burkart, A., Cilia, C., Cogliati, S., Colombo, R., Damm, A., Drusch, M., Guanter, L., Hanus, J., et al., 2015. Sun-induced fluorescence — a new probe of photosynthesis: first maps from the imaging spectrometer HyPlant. Glob. Chang. Biol. 21 (12), 4673–4684.

Rosema, A., Snel, J., Zahn, H., Buurmeijer, W., Van Hove, L., 1998. The relation between laser-induced chlorophyll fluorescence and photosynthesis. Remote Sens. Environ. 65 (2), 143–154.
Rossini, M., Nedbal, L., Guanter, L., Ač, A., Alonso, L., Burkart, A., Cogliati, S., Colombo, R., Damm, A., Drusch, M., et al., 2015. Red and far red sun-induced chlorophyll fluorescence as a measure of plant photosynthesis. Geophys. Res. Lett. 42 (6), 1632–1639.
Rouse Jr, J.W., Haas, R.H., Schell, J., Deering, D., 1973. Monitoring the vernal advancement and retrogradation (green wave effect) of natural vegetation. In: NASA report.
Sabater, N., Vicent, J., Alonso, L., Verrelst, J., Middleton, E., Porcar-Castell, A., Moreno, J., 2018. Compensation of oxygen transmittance effects for proximal sensing retrieval of canopy-leaving sun-induced chlorophyll fluorescence. Remote Sens. 10 (10), 1551.
Schreiber, U., 1998. Chlorophyll fluorescence: new instruments for special applications. In: Photosynthesis: Mechanisms and Effects. Springer, pp. 4253–4258.
Schreiber, U., Schliwa, U., Bilger, W., 1986. Continuous recording of photochemical and non-photochemical chlorophyll fluorescence quenching with a new type of modulation fluorometer. Photosynth. Res. 10 (1-2), 51–62.
Schull, M., Ganguly, S., Samanta, A., Huang, D., Shabanov, N., Jenkins, J., Chiu, J.C., Marshak, A., Blair, J., Myneni, R., et al., 2007. Physical interpretation of the correlation between multi-angle spectral data and canopy height. Geophys. Res. Lett. 34 (18).
Shan, N., Ju, W., Migliavacca, M., Martini, D., Guanter, L., Chen, J., Goulas, Y., Zhang, Y., 2019. Modeling canopy conductance and transpiration from solar-induced chlorophyll fluorescence. Agric. For. Meteorol. 268, 189–201.
Smolander, S., Stenberg, P., 2005. Simple parameterizations of the radiation budget of uniform broadleaved and coniferous canopies. Remote Sens. Environ. 94 (3), 355–363.
Stenberg, P., M ottus, M., Rautiainen, M., 2016. Photon recollision probability in modelling the radiation regime of canopies — a review. Remote Sens. Environ. 183, 98–108.
Tucker, C.J., 1979. Red and Photographic Infrared Linear Combinations for Monitoring Vegetation. 150. pp. 127–150.
Van der Tol, C., Verhoef, W., Timmermans, J., Verhoef, A., Su, Z., 2009. An integrated model of soil-canopy spectral radiances, photosynthesis, fluorescence, temperature and energy balance. Biogeosciences 6 (12), 3109–3129.
Van der Tol, C., Berry, J., Campbell, P., Rascher, U., 2014. Models of fluorescence and photosynthesis for interpreting measurements of solar-induced chlorophyll fluorescence. J. Geophys. Res. Biogeo. 119 (12), 2312–2327.
Van der Tol, C., Rossini, M., Cogliati, S., Verhoef, W., Colombo, R., Rascher, U., Mohammed, G., 2016. A model and measurement comparison of diurnal cycles of sun-induced chlorophyll fluorescence of crops. Remote Sens. Environ. 186, 663–677.
Van der Tol, C., Vilfan, N., Dauwe, D., Cendrero-Mateo, M.P., Yang, P., 2019. The scattering and re-absorption of red and near-infrared chlorophyll fluorescence in the models Fluspect and SCOPE. Remote Sens. Environ. 232, 111292.
Van Wittenberghe, S., Alonso, L., Verrelst, J., Moreno, J., Samson, R., 2015. Bidirectional sun-induced chlorophyll fluorescence emission is influenced by leaf structure and light scattering properties — a bottom-up approach. Remote Sens. Environ. 158, 169–179.
Verrelst, J., Rivera, J.P., van der Tol, C., Magnani, F., Mohammed, G., Moreno, J., 2015. Global sensitivity analysis of the SCOPE model: what drives simulated canopy-leaving sun-induced fluorescence? Remote Sens. Environ. 166, 8–21.
Verrelst, J., Malenovskỳ, Z., Van der Tol, C., Camps-Valls, G., Gastellu-Etchegorry, J.-P., Lewis, P., North, P., Moreno, J., 2019. Quantifying vegetation biophysical variables from imaging spectroscopy data: a review on retrieval methods. Surv. Geophys. 40 (3), 589–629.
Viña, A., Gitelson, A.A., 2005. New developments in the remote estimation of the fraction of absorbed photosynthetically active radiation in crops. Geophys. Res. Lett. 32 (17).
Wiegand, C.L., 1977. Distinguishing Vegetation from Soil Background Information. 43 (12). pp. 1541–1552.
Wieneke, S., Burkart, A., Cendrero-Mateo, M., Julitta, T., Rossini, M., Schickling, A., Schmidt, M., Rascher, U., 2018. Linking photosynthesis and sun-induced fluorescence at sub-daily to seasonal scales. Remote Sens. Environ. 219, 247–258.
Wohlfahrt, G., Gerdel, K., Migliavacca, M., Rotenberg, E., Tatarinov, F., Müller, J., Hammerle, A., Julitta, T., Spielmann, F., Yakir, D., 2018. Sun-induced fluorescence and gross primary productivity during a heat wave. Sci. Rep. 8 (1), 14169.
Yang, P., Van der Tol, C., 2018. Linking canopy scattering of far-red sun-induced chlorophyll fluorescence with reflectance. Remote Sens. Environ. 209, 456–467.
Yang, X., Tang, J., Mustard, J.F., Lee, J.-E., Rossini, M., Joiner, J., Munger, J.W., Kornfeld, A., Richardson, A.D., 2015. Solar-induced chlorophyll fluorescence that correlates with canopy photosynthesis on diurnal and seasonal scales in a temperate deciduous forest. Geophys. Res. Lett. 42 (8), 2977–2987.
Yang, H., Yang, X., Zhang, Y., Heskel, M.A., Lu, X., Munger, J.W., Sun, S., Tang, J., 2017a. Chlorophyll fluorescence tracks seasonal variations of photosynthesis from leaf to canopy in a temperate forest. Glob. Chang. Biol. 23 (7), 2874–2886.
Yang, P., Verhoef, W., van der Tol, C., 2017b. The mSCOPE model: a simple adaptation to the SCOPE model to describe reflectance, fluorescence and photosynthesis of vertically heterogeneous canopies. Remote Sens. Environ. 201, 1–11.
Yang, K., Ryu, Y., Dechant, B., Berry, J.A., Hwang, Y., Jiang, C., Kang, M., Kim, J., Kimm, H., Kornfeld, A., et al., 2018. Sun-induced chlorophyll fluorescence is more strongly related to absorbed light than to photosynthesis at half-hourly resolution in a rice paddy. Remote Sens. Environ. 216, 658–673.
Yang, P., van der Tol, C., Verhoef, W., Damm, A., Schickling, A., Kraska, T., Muller, O., Rascher, U., 2019. Using reflectance to explain vegetation biochemical and structural effects on sun-induced chlorophyll fluorescence. Remote Sens. Environ. 231, 110996.
Yoshida, Y., Joiner, J., Tucker, C., Berry, J., Lee, J.-E., Walker, G., Reichle, R., Koster, R., Lyapustin, A., Wang, Y., 2015. The 2010 Russian drought impact on satellite measurements of solar-induced chlorophyll fluorescence: insights from modeling and comparisons with parameters derived from satellite reflectances. Remote Sens. Environ. 166, 163–177.
Zeng, Y., Badgley, G., Dechant, B., Ryu, Y., Chen, M., Berry, J.A., 2019. A practical approach for estimating the escape ratio of near-infrared solar-induced chlorophyll fluorescence. Remote Sens. Environ. 232, 111209.
Zhang, Q., Cheng, Y.-B., Lyapustin, A.I., Wang, Y., Gao, F., Suyker, A., Verma, S., Middleton, E.M., 2014. Estimation of crop gross primary production (GPP): fAPARchl versus MOD15A2 FPAR. Remote Sens. Environ. 153, 1–6.
Zhang, Q., Middleton, E.M., Cheng, Y.-B., Huemmrich, K.F., Cook, B.D., Corp, L.A., Kustas, W.P., Russ, A.L., Prueger, J.H., Yao, T., 2016. Integrating chlorophyll fAPAR and nadir photochemical reflectance index from EO-1/Hyperion to predict cornfield daily gross primary production. Remote Sens. Environ. 186, 311–321.

Fluorescence Correction Vegetation Index (FCVI): A physically based reflectance index to separate physiological and non-physiological information in far-red sun-induced chlorophyll fluorescence

Peiqi Yang*, Christiaan van der Tol, Petya K. E. Campbell, Elizabeth M. Middleton

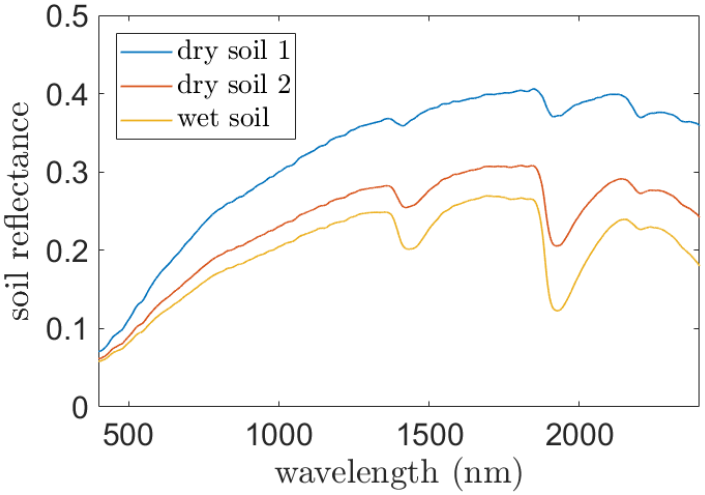

Figure S1. Soil reflectance in the SCOPE simulations.

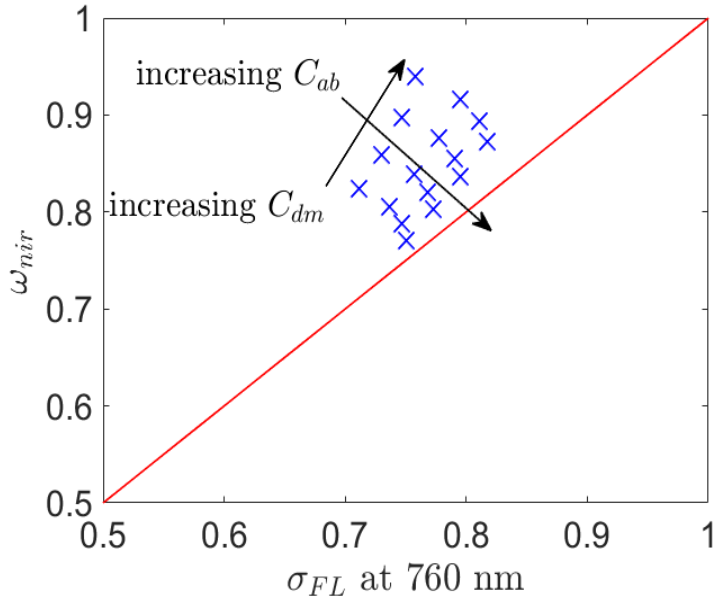

Figure S2. Comparison of within-leaf scattering of fluorescence at 760 nm (σ_{FL}) and leaf albedo at 760 nm. The data are simulated using the FLUSPECT model varying leaf dry matter (Cdm) and chlorophyll content (Cab).

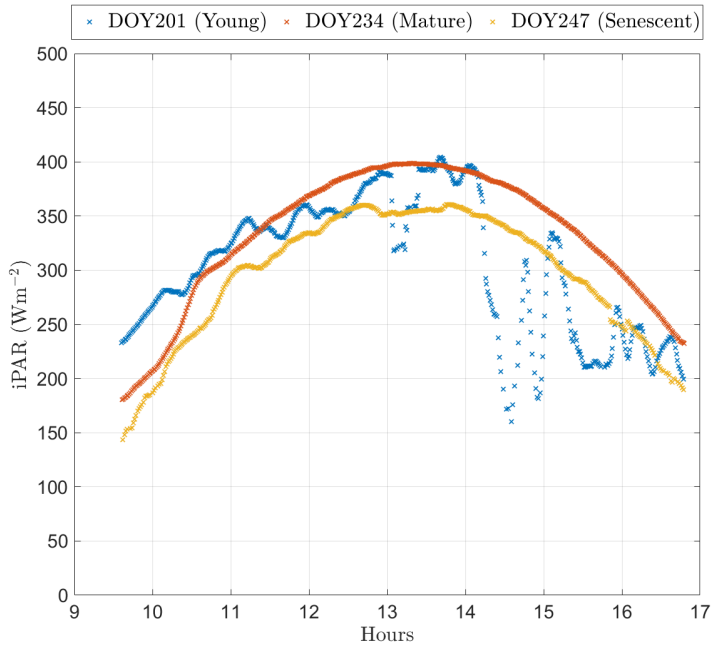

Figure S3. Diurnal variations of iPAR on one sunny day representative for each growth stage.

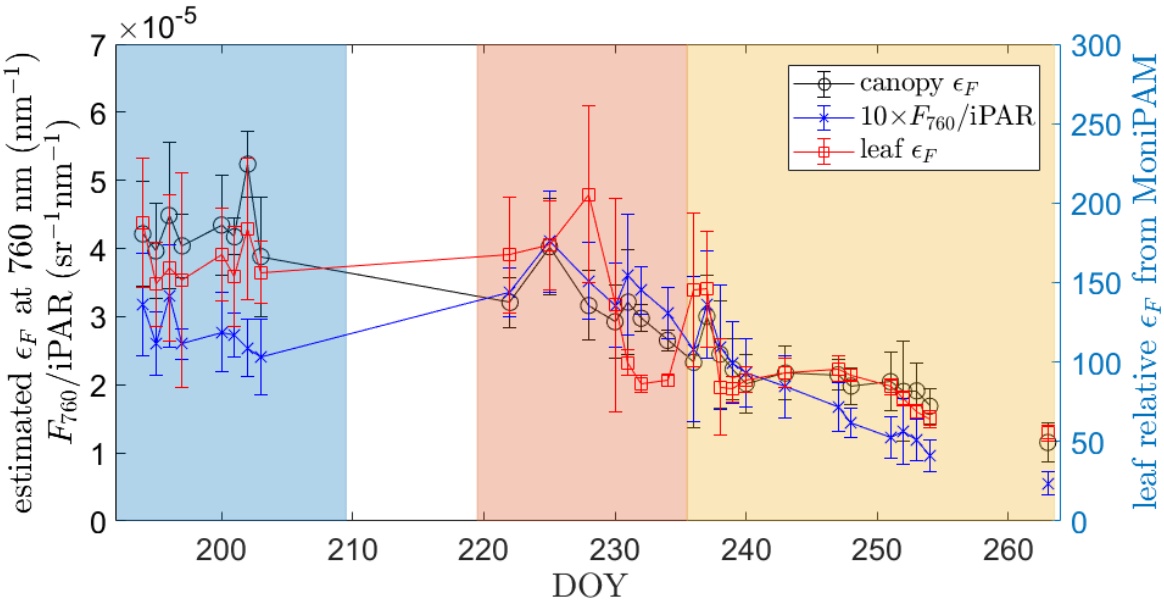

Figure S4. Comparison between estimated canopy fluorescence emission efficiency from TOC reflectance and SIF measurements and leaf relative fluorescence emission efficiency measured by MoniPAM at middays on sunny or partly cloudy days in the growing season.

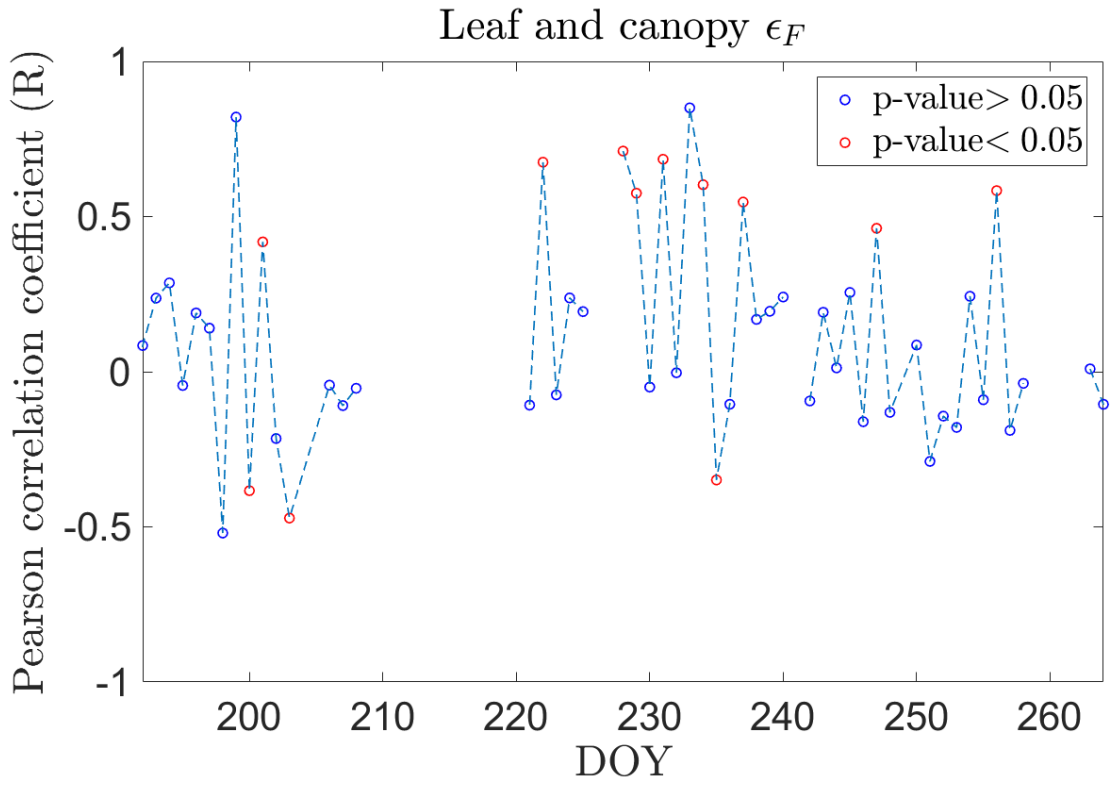

Figure S5. Pearson correlation coefficient (R) between leaf and canopy ϵ_F on individual days.

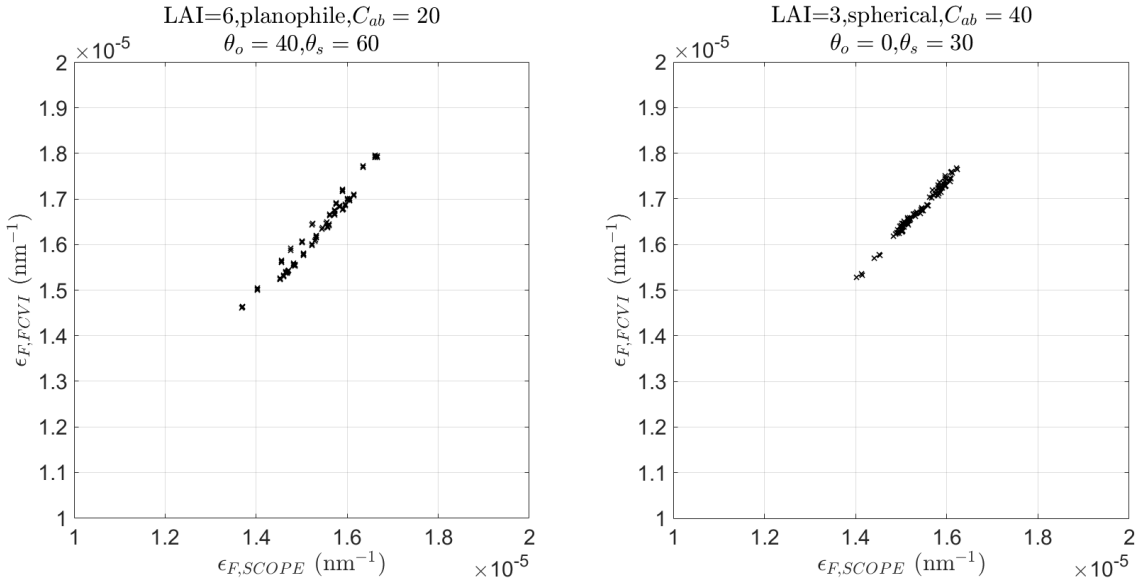

Figure S6. Comparison between fluorescence emission efficiency used in SCOPE and estimated fluorescence emission efficiency from top-of-canopy reflectance and SIF measurements of the synthetic scenarios. Two subsets from Fig. 8b in the paper.

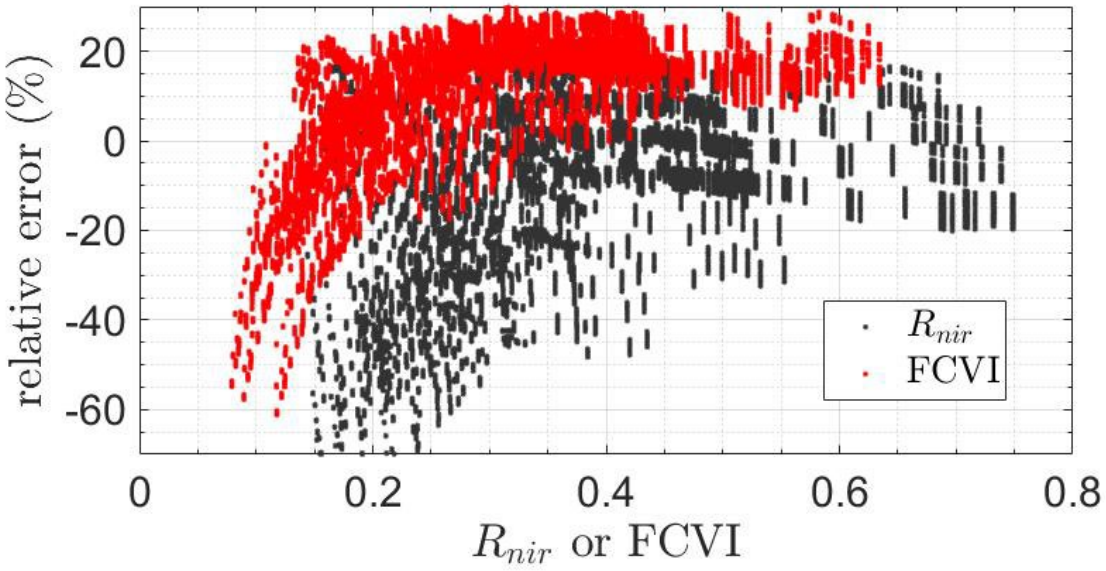

Fig. S7. The relative error of using Rnir and FCVI to estimate ϵ_F of real soil scenarios as a comparison to Fig. 8d in the paper.

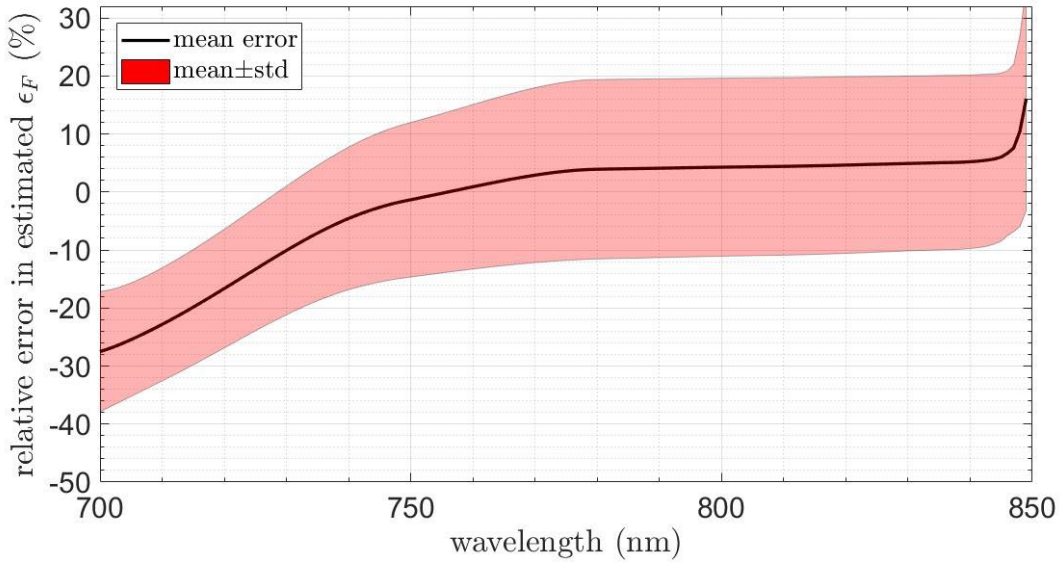

Fig. S8. The relative error of using FCVI to estimate ϵ_F of real soil scenarios for far-red SIF at different wavelength. The scenarios presented in Fig. 8b and 8d

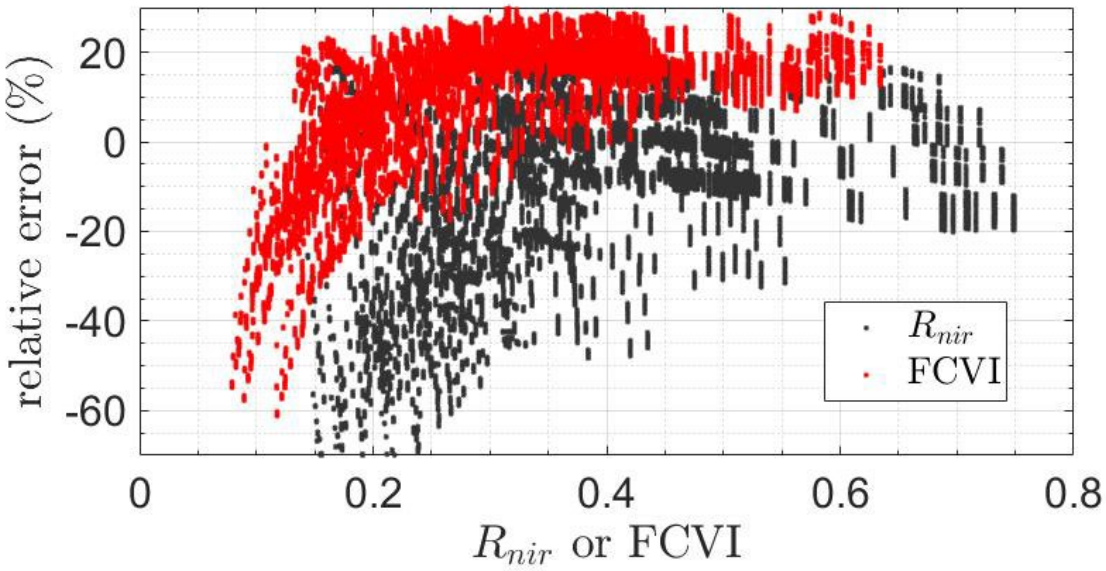

are used here.